12-2012

Flow Characteristics of Arced Labyrinth Weirs

Nathan A. Christensen

FLOW CHARACTERISTICS OF

ARCED LABYRINTH WEIRS

by

Nathan A. Christensen

A thesis submitted in partial fulfillment
of the requirements for the degree

of

MASTER OF SCIENCE

in

Civil and Environmental Engineering

Approved:

Blake P. Tullis Major Professor	Brian M. Crookston Committee Member
John D. Rice Committee Member	Mark R. McLellan Vice President for Research and Dean of the School of Graduate Studies

UTAH STATE UNIVERSITY
Logan, Utah

2012

ABSTRACT

Flow Characteristics of Arced Labyrinth Weirs

by

Nathan A. Christensen, Master of Science

Utah State University, 2012

Major Professor: Blake P. Tullis
Department: Civil and Environmental Engineering

The need to accommodate larger reservoir discharge events has prompted the improvement or replacement of existing spillways. One possible spillway modification is the use of an in-reservoir arced labyrinth weir in place of a linear weir. Arced labyrinth weirs can increase crest length (more cycles) and have improved hydraulic efficiency in non-channelized approach flow applications, compared to traditional labyrinth weir applications.

In this study, arced labyrinth weir flow characteristics were observed for eleven different laboratory-scale model geometries at the Utah Water Research Laboratory. Rating (C_d vs. H_T/P) data and observations were recorded for each configuration, and discharge efficiency was determined. Cycle efficiency, which is representative of the discharge per cycle, was also reported.

In-reservoir labyrinth weirs with larger sidewall angles ($\geq 20°$) were found to have higher discharge efficiency than in-reservoir weirs with smaller sidewall angles ($< 20°$). On the other hand, arced labyrinth weirs with longer crest length (occurring on

geometries with $\alpha < 20°$) were more efficient per cycle than $\alpha = 20°$ weirs. Aeration characteristics, inlet modification options, weir placement options, and nappe breakers were also investigated for arced and non-arced labyrinth weirs (in-reservoir).

As the upstream head increases, the outlet cycles of the arced labyrinth weirs experience local submergence (beginning at the upstream apex region). Eventually, the entire weir structure can become submerged when the inflow exceeds the weir's free-flow discharge capacity. When this occurs, the head-discharge control point can move to a location downstream of the weir. Larger cycle arc angles (θ) are more susceptible to this phenomenon. Flow separation also contributed to decreased capacity at higher discharges (higher heads). Adding cycles to the weir length (from 5 cycles to 7 and 10 cycles) was also found to have slight to negligible effect on discharge efficiency, but due to increased weir length, discharge increased proportionally.

No current design method exists for arced labyrinth weirs, and limited hydraulic data (specific to arced labyrinth weirs) is currently available. This study continues the dialogue for arced labyrinth weir hydraulics and increases the repository of data available for their design. This data may be used, with sound engineering judgment, to better understand the flow characteristics of arced labyrinth weirs.

(106 pages)

PUBLIC ABSTRACT

Flow Characteristics of Arced Labyrinth Weirs

by

Nathan A. Christensen, Master of Science

Utah State University, 2012

Major Professor: Blake P. Tullis
Department: Civil and Environmental Engineering

The need to accommodate larger reservoir discharge events has prompted the improvement or replacement of existing spillways. One possible spillway modification is the use of an in-reservoir arced labyrinth weir in place of a linear weir. Arced labyrinth weirs can increase crest length (more cycles) and have improved hydraulic efficiency in non-channelized approach flow applications, compared to traditional labyrinth weir applications.

In this study, arced labyrinth weir flow characteristics were observed for eleven different laboratory-scale model geometries at the Utah Water Research Laboratory. Rating (C_d vs. H_T/P) data and observations were recorded for each configuration, and discharge efficiency was determined. Cycle efficiency, which is representative of the discharge per cycle, was also reported.

In-reservoir labyrinth weirs with larger sidewall angles ($\geq 20°$) were found to have higher discharge efficiency than in-reservoir weirs with smaller sidewall angles ($< 20°$). On the other hand, arced labyrinth weirs with longer crest length (occurring on

geometries with $\alpha < 20°$) were more efficient per cycle than $\alpha = 20°$ weirs. Aeration characteristics, inlet modification options, weir placement options, and nappe breakers were also investigated for arced and non-arced labyrinth weirs (in-reservoir).

As the upstream head increases, the outlet cycles of the arced labyrinth weirs experience local submergence (beginning at the upstream apex region). Eventually, the entire weir structure can become submerged when the inflow exceeds the weir's free-flow discharge capacity. When this occurs, the head-discharge control point can move to a location downstream of the weir. Larger cycle arc angles (θ) are more susceptible to this phenomenon. Flow separation also contributed to decreased capacity at higher discharges (higher heads). Adding cycles to the weir length (from 5 cycles to 7 and 10 cycles) was also found to have slight to negligible effect on discharge efficiency, but due to increased weir length, discharge increased proportionally.

No current design method exists for arced labyrinth weirs, and limited hydraulic data (specific to arced labyrinth weirs) is currently available. This study continues the dialogue for arced labyrinth weir hydraulics and increases the repository of data available for their design. This data may be used, with sound engineering judgment, to better understand the flow characteristics of arced labyrinth weirs.

ACKNOWLEDGMENTS

This study has been a great experience for me. There are several people who deserve much thanks and appreciation for making it all possible. I would first like to acknowledge Mac McKee for approving the funding for this project. I'm also very thankful to my graduate advisor, Blake Tullis, for the important insights, ideas, approvals, and support he has given me throughout this study. My other committee members, Brian Crookston and John Rice, deserve great thanks for their suggestions, input, and direction.

There are also several people who gave me support and help while building models, collecting data, and running water. Thanks to Zac Sharp and the hydraulics lab staff for always helping me build as needed. Thanks to Mitch Dabling, Riley Olsen, Nate Decker, Nate Wright, and Amber Olsen for helping level and/or take crest references on several models. I would like to give special acknowledgment to Ricky Anderson and Mitch Dabling for the countless hours spent building and installing weirs, and for getting glue on their clothes.

Finally, I'd like to thank my family for their encouragement, my friends for giving me up to late nights, and most especially God for giving me strength to move forward. I'd say everything has been a success!

Nathan A. Christensen

CONTENTS

Page

ABSTRACT iii

PUBLIC ABSTRACT v

ACKNOWLEDGMENTS vii

LIST OF TABLES x

LIST OF FIGURES xi

NOMENCLATURE xi

INTRODUCTION 1

LITERATURE REVIEW 4

- Arced Labyrinth Weirs 4
- Flow Characteristics 8
- Research Objectives 11

EXPERIMENTAL SETUP 13

- Test Facilities 13
- Labyrinth Weir Model Fabrication and Installation 15
- Instrumentation 18

TESTING PROCEDURE 22

EXPERIMENTAL RESULTS AND DISCUSSION 25

- Sidewall Angle Effects 27
- Cycle Efficiency 37
- Cycle Arcing Effects 37
- Approach Flow Velocity Field 40
- Arced Labyrinth and Arced Linear Weir Comparison 41
- Abutment Effects 42
- Cycle Number Comparisons 44
- Sources of Error & Uncertainty 46

APPLICATION OF RESULTS 48

CONCLUSIONS & RECOMMENDATIONS 50

REFERENCES 52

APPENDICES 55

APPENDIX A: Drawings & Photographs 56
APPENDIX B: Data 70
APPENDIX C: Microsoft Excel VBA Code 84

LIST OF TABLES

Table		Page
1	List of models tested in US units	23
2	Trend line coefficients for half round crests	26
3	Head-discharge control point shift using Q_{Lab} and Q_{Lin}	42
B1	10-cycle, α = 12°, θ = 10° data	71
B2	7-cycle, α = 12°, θ = 10° data	72
B3	5-cycle, α = 12°, θ = 20° data	73
B4	5-cycle, α = 12°, θ = 10° data	74
B5	10-cycle, α = 20°, θ = 10° data	75
B6	5-cycle, α = 20°, θ = 30° data	76
B7	5-cycle, α = 20°, θ = 20° data	77
B8	5-cycle, α = 20°, θ = 10° data	78
B9	5-cycle, α = 20°, θ = 0°, projecting data	79
B10	5-cycle, α = 20°, θ = 0°, flush data	80
B11	5-cycle, α = 20°, θ = 0°, rounded inlet data	81

LIST OF FIGURES

Figure		Page
1	Linear & labyrinth weir	2
2	Example of prototype labyrinth weir	3
3	10-cycle arced labyrinth weir configuration	6
4	Crookston (2010) arced vs. non arced labyrinth weirs	7
5	Weir placement & abutment types	11
6	UWRL & reservoir/headbox	13
7	20-inch (50.8 cm) supply line with mag-meters	14
8	6-inch (15.2 cm) supply line with mag-meters	14
9	Plenum chamber with diffuser pipe and baffled wall	15
10	Half-round crest weir wall	16
11	Removable walls for changing width (*W)*	17
12	Surveying & leveling	18
13	Multi-meter attached to mag-meter	19
14	Stilling basin & point gauge	20
15	Velocity probe & dye wand injection	21
16	Summary schematic of models tested	22
17	Nappe breakers	24
18	Sidewall angle α = 12° discharge data with curve fits	25
19	Sidewall angle α = 20° discharge data with curve fits	26
20	Nappe aeration conditions for α = 20° sidewall angle	28

21 Nappe aeration conditions for α = 12° sidewall angle 28

22 Half-round aeration conditions and terms..... 29

23 Natural aeration of 1.5 cycles on α = 12° sidewalls (H_T/P = 0.2)..... 30

24 Natural aeration of 0.5 cycles on α = 20° sidewalls (H_T/P = 0.2)..... 30

25 Artificial nappe aeration C_d data normalized by the natural nappe aeration condition (no nappe breakers) (α = 20°) 32

26 Artificial nappe aeration C_d data normalized by the natural nappe aeration condition (no nappe breakers) (α = 12°) 32

27 Artificial aeration on α = 20° sidewalls (H_T/P = 0.2) 33

28 Local submergence at 0.3 H_T/P on α = 12° sidewall angle..... 34

29 Local submergence at 0.3 H_T/P on α = 20° sidewall angle..... 34

30 Arced weir in-reservoir compared to non-arced weir in-channel, α = 6° . 35

31 Arced weir in-reservoir compared to non-arced weir in-channel, α = 12° 36

32 Arced weir in-reservoir compared to non-arced weir in-channel, α = 20° 36

33 Cycle efficiency vs. head 38

34 Arced weir compared to non-arced weir in-reservoir for α = 12° 39

35 Arced weir compared to non-arced weir in-reservoir for α = 20° 39

36 Head-discharge control point shift, H_T/P = 0.3 (grey) and H_T/P = 0.6 (black) 40

37 Arced linear weir (R = 2.58 ft) overlaid on an arced labyrinth weir (5-cycle, α = 20°, R = 2.58 ft) 41

38 Comparison of inlet modifications on various sidewall angles 43

39 Projecting weir (Left) vs. rounded inlet weir (Right) at H_T/P = 0.3 44

40 C_d data for θ = 10° (α = 12° and 20°) weirs with 5, 7, and 10 cycles..... 45

41 Q vs. H_T (N emphasized) for all models 46

42 Q vs. H_T (α emphasized) for all models 48

43 Q vs. H_T (θ emphasized) for all models 49

A1 Headbox 2D elevation schematic 57

A2 Headbox 3D schematic 58

A3 10-cycle, α = 12°, θ = 10°, schematic 59

A4 10-cycle, α = 12°, θ = 10°, photograph 59

A5 7-cycle, α = 12°, θ = 10°, schematic 60

A6 7-cycle, α = 12°, θ = 10°, photograph 60

A7 5-cycle, α = 12°, θ = 20°, schematic 61

A8 5-cycle, α = 12°, θ = 20°, photograph 61

A9 5-cycle, α = 12°, θ = 10°, schematic 62

A10 5-cycle, α = 12°, θ = 10°, photograph 62

A11 10-cycle, α = 20°, θ = 10°, schematic 63

A12 10-cycle, α = 20°, θ = 10°, photograph 63

A13 5-cycle, α = 20°, θ = 30°, schematic 64

A14 5-cycle, α = 20°, θ = 30°, photograph 64

A15 5-cycle, α = 20°, θ = 20°, schematic 65

A16 5-cycle, α = 20°, θ = 20°, photograph 65

A17 5-cycle, α = 20°, θ = 10°, schematic 66

A18 5-cycle, α = 20°, θ = 10°, photograph 66

A19 5-cycle, α = 20°, θ = 0° projecting, schematic 67

A20 5-cycle, α = 20°, θ = 0° projecting, photograph 67

A21 5-cycle, α = 20°, θ = 0° flush, schematic 68

A22 5-cycle, α = 20°, θ = 0° flush, photograph 68

A23 5-cycle, α = 20°, θ = 0° rounded inlet, schematic 69

A24 5-cycle, α = 20°, θ = 0° rounded inlet, photograph 69

B1 10-cycle, α = 12º, θ = 10º velocity grid at H_T/P = 0.3 82

B2 5-cycle, α = 12º, θ = 10º velocity grid at H_T/P = 0.3 82

B3 5-cycle, α = 20º, θ = 20º velocity grid at H_T/P = 0.3 83

B4 5-cycle, α = 20º, θ = 20º velocity grid at H_T/P = 0.6 83

NOMENCLATURE

A_c	Apex centerline width
α	Sidewall angle
α'	Upstream sidewall angle, $\alpha' = \alpha + \theta/2$
C_d	Discharge coefficient
$C_{d\text{-}arced}$	Discharge coefficient for an arced projecting labyrinth weir in a reservoir
$C_{d\text{-}artificial}$	Discharge coefficient for an arced labyrinth weir artificially aerated
$C_{d\text{-}channel}$	Discharge coefficient for a labyrinth weir in a channel
$C_{d\text{-}natural}$	Discharge coefficient for an arced labyrinth weir naturally aerated
$C_{d\text{-}projecting}$	Discharge coefficient for a linear projecting labyrinth weir in a reservoir
$C_{d\text{-}res}$	Discharge coefficient for a labyrinth weir in a reservoir
ε'	Cycle efficiency, $\varepsilon' = C_d * L_{c\text{-}cycle}/w$
g	Acceleration of gravity
h	Depth of flow over weir crest
H_T	Total head
H_T/P	Headwater ratio
l_c	Centerline length of sidewall
L_c	Centerline length of weir, $L_c = L_{c\text{-}cycle} * N$
$L_{c\text{-}cycle}$	Centerline length of one complete cycle
N	Number of cycles
ω_{H_T}	Uncertainty interval for total head
ω_{L_c}	Uncertainty interval for centerline crest length

ω_P	Uncertainty interval for weir height
ω_Q	Uncertainty interval for flow rate
ω_W	Uncertainty interval for channel width
P	Weir height
Q	Discharge
Q_{Lab}	Discharge over arced labyrinth weir
Q_{Lin}	Discharge over arced linear weir
r	Segment height from channel opening to center of imaginary arc circle
r'	Segment height from channel opening to perpendicular downstream apex
R	Arc radius, $R = (W^2/4 + r'^2)^{1/2}$
R_{crest}	Radius of crest shape
θ	Cycle arc angle, $\theta = \Theta/N$
Θ	Central arc angle, $\Theta = W'/R$
t_w	Wall thickness at crest
V_{up}	Approach velocity
w	Cycle width for a labyrinth weir
w'	Cycle arc width, $w' = W'/N$
W	Downstream channel width
W'	Arced labyrinth weir arc width ($R\Theta$)

INTRODUCTION

Weirs are hydraulic structures used for measuring flow rate; controlling flood water; providing water storage, grade control, and flow diversion; and altering flow regime in a channel or river. Weirs are also commonly used as control structures for dam spillways. Revisions of probable maximum flood events (PMF) have created a growing need to increase discharge capacity for existing dams.

Flow over a weir can be described empirically with a standard form of the weir head-discharge equation (Eq. [1]) (Henderson 1966). In this equation, Q is the flow over the crest, H_T is the total measured head relative to the crest elevation, L_c is the centerline weir crest length, C_d the discharge coefficient, and g the acceleration constant of gravity.

$$Q = C_d \frac{2}{3} L_c {H_T}^{3/2} \sqrt{2g} \qquad [1]$$

Per Eq. [1], discharge is directly proportional to L_c. Since the width of the channel or reservoir in which a weir is installed is often restricted, one way to increase discharge capacity is to increase L_c by folding the weir (in plan-view) into trapezoidal segments or cycles, creating a nonlinear or 3-D weir, referred to as a labyrinth weir (Fig. 1). Labyrinth weir hydraulics were first investigated by Gentilini (1940). A prototype version of a labyrinth weir is seen in Fig. 2.

Kocahan and Taylor (2002) suggested that the labyrinth-shaped weir allows more discharge than a regular ogee weir at the beginning of a flood and doesn't depend on "mechanical equipment or human intervention" (i.e., passive control). Increasing the weir length (and subsequently Q) of an existing spillway channel by replacing a linear

weir with a labyrinth weir represents, in most cases, a more economical and efficient alternative relative to widening the spillway channel (Tullis et al. 1995). They have also been successfully used as in-channel energy dissipaters and flow aeration structures (Crookston 2010).

Labyrinth weir research has continued for decades, with contributions from Taylor (1968), Hay and Taylor (1970), Darvas (1971), Houston (1982), Hinchliff and Houston (1984), Lux (1984), Megalhaes (1985), Tullis, J. P. (1992), Tullis, J. P. et al. (1995), Savage et al. (2004), Tullis, B. and Young (2005), Lopes et al. (2008), Tullis, B. et al. (2007), and Crookston and Tullis, B. (2012 a, b, c). The hydraulic design methods and case studies in this literature have contributed to the research in this study and show that labyrinth weirs are both versatile and adaptable.

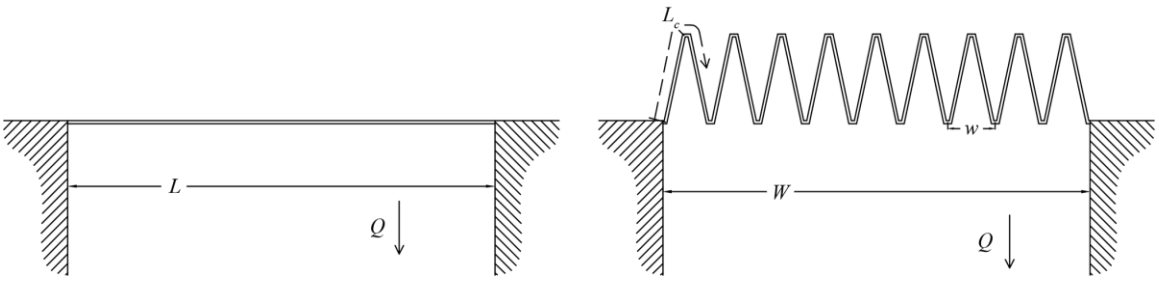

Fig. 1. Linear & labyrinth weir.

Fig. 2. Example of prototype labyrinth weir.
(Yahoola Dam, Georgia. Photo courtesy of Schnabel Engineering)

LITERATURE REVIEW

Arced Labyrinth Weirs

In reservoir applications, labyrinth weirs can be modified to orient the cycles to non-channelized approach flows. A cycle layout where the downstream apexes follow the arc of a circle is termed an arced labyrinth weir.

Previous model studies have shown arced or radial labyrinth weirs to be viable options for reservoir-weir applications where approach flow conditions are non-channelized. Copeland and Fletcher (2000) have stated that "the spillway capacity of a labyrinth weir is sensitive to both the magnitude and direction of approach flows." Yildiz and Uzecek (1996) determined that arced labyrinth discharge could be as much as twice that of a classical labyrinth spillway due to better flow accommodation. Non-channelized approach flow conditions have led to increased discharge capacity in some reservoir settings. Houston's (1983) data supports this idea when it shows that a weir projecting into a reservoir has approximately 20% larger discharge than a similar in-channel labyrinth weir at comparable heads.

Falvey (2003) cited Prado spillway, near Corona, CA, as an example where the approach flow conditions to the labyrinth play an important role in determining discharge capacity. That publication explains that if the cycle alignment had been curved, the discharge coefficient would have been higher. To support this point, Falvey (2003) identified three additional model studies (Kizilcapinar, Sarioglan, and Avon spillways) that were impacted by non-ideal approach flow conditions. These problems included: lower discharge capacity, turbulent flow over the crest, and uneven nappe aeration. The

Kizilcapinar and Avon labyrinth weir designs were eventually arced in an effort to address some of these concerns and improve discharge efficiency. For Maria Cristina Dam (Spain), the approach flow conditions and discharge capacity could be improved by arcing the labyrinth weir within the limited footprint area of the spillway (Cordero Page et al. 2007). A seven-cycle labyrinth weir, with six cycles arced, was selected as the optimal design (Cordero Page et al. 2007). These arced labyrinth weir case studies demonstrate the usefulness of these types of labyrinth weirs and the merit of additional hydraulic research.

Based on laboratory experiments of labyrinth weirs in reservoir applications, Crookston (2010) concluded that "the arced configurations were found to be the most efficient labyrinth weirs tested" and that "an arced cycle configuration can increase discharge efficiency as it improves the orientation of the cycle to the approaching flow (~90° to the weir centerline is desirable)." Crookston and Tullis (2012a) introduced geometric parameter nomenclature specific to arced labyrinth weirs as shown in Fig. 3; that nomenclature was adopted for this study.

Arced labyrinth weir geometric parameters include:

α	Sidewall angle (used for linear or arced configurations)
α'	Upstream sidewall angle, $\alpha' = \alpha + \theta/2$
L_c	Centerline length of weir
$L_{c\text{-}cycle}$	Centerline length of one complete cycle
l_c	Centerline length of the sidewall
N	Number of cycles or trapezoidal folds
Q	Flow

r'	Segment height from channel opening to perpendicular downstream apex
r	Segment height from channel opening to center of imaginary arc circle
R	Arc radius, $R = (W^2/4 + r'^2)^{1/2}$
θ	Cycle arc angle, $\theta = \Theta/N$
Θ	Central arc angle, $\Theta = W'/R$
t_w	Wall thickness at crest
w'	Cycle arc width, $w' = W'/N$
W	Downstream channel width

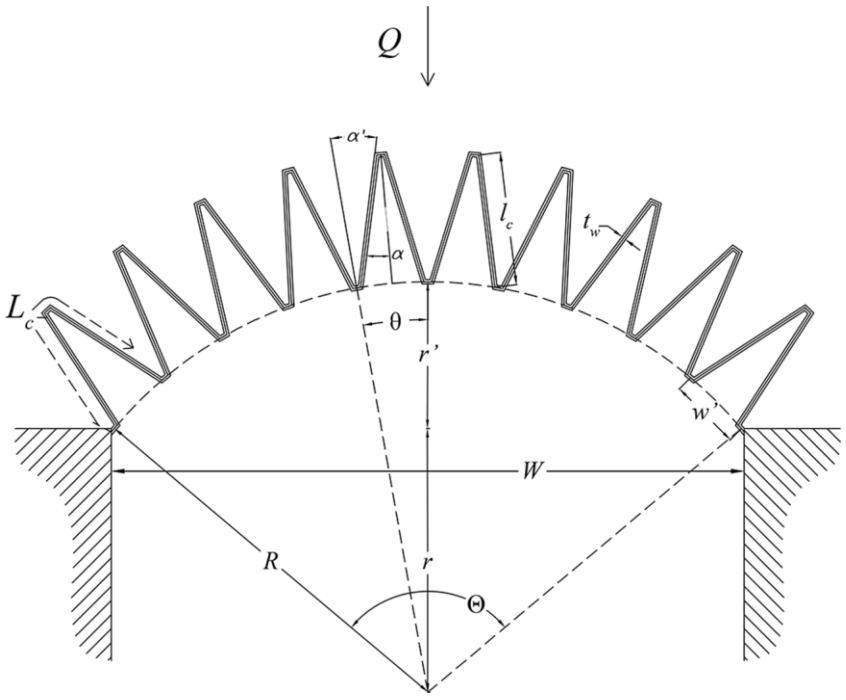

Fig. 3. 10-cycle arced labyrinth weir configuration.

For a given channel width (W), arced flow characteristics vary with cycle number (N), arc radius (R), upstream and downstream cycle sidewall angles (α and α', respectively), cycle arc angle (θ), weir thickness (t_w), and apex geometry. The influence of various arced labyrinth weir geometric variations has thus far been accounted for via the experimentally determined C_d (Eq. [1]). This coefficient is an indicator of weir unit-width discharge, referred to as hydraulic efficiency, for different configurations. Geometry-specific C_d data vs. H_T/P regression equations can be produced for easier application of Eq. [1] in design. The C_d data in Fig. 4 represent a snapshot of the Crookston (2010) α = 6° arced and non-arced labyrinth weir data.

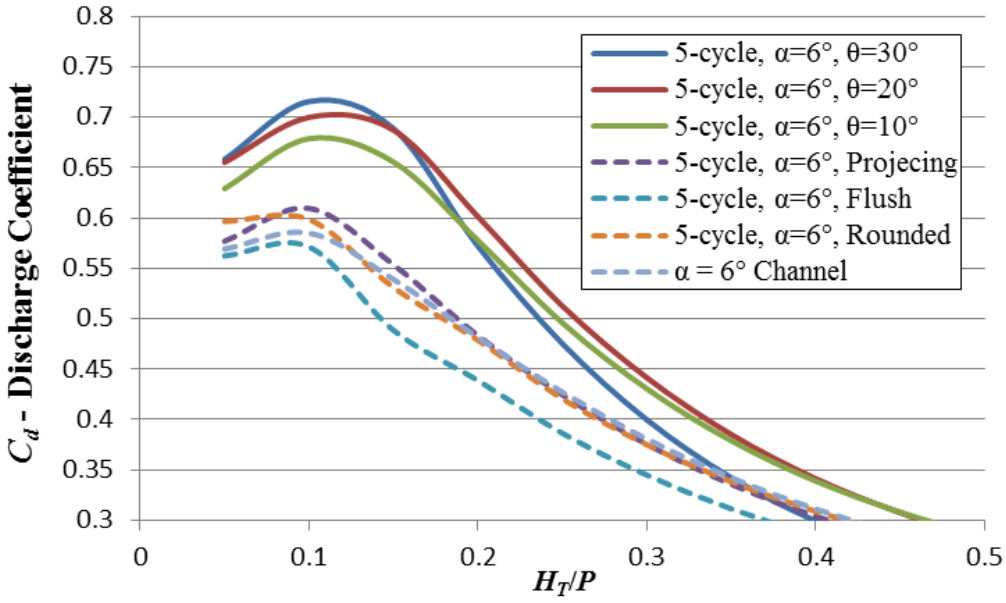

Fig. 4. Crookston (2010) arced vs. non arced labyrinth weirs.

These data show that arced labyrinth weirs are (under specific in-situ flow characteristics) more efficient than non-arced weirs in a reservoir. Wilson (1995) touched on this when he stated, "the radial design of the labyrinth was dictated by the

need to conduct flows efficiently from the labyrinth to a point destination." Arced labyrinth weir hydraulic efficiency is directly affected by site-specific flow characteristics. These characteristics (i.e. poor flow conductance, increased nappe instability, and increased local submergence) directly impact discharge efficiency (Crookston 2010). It is also important to note that under differing site conditions, Tacail et al. (1990) found that the semicircular or arced labyrinth weir created only the same approximate discharge at maximum head as non-arced weirs (specific to his test conditions).

In response, Crookston (2010) explored the effects of arced labyrinth weir geometry on discharge efficiency. The geometric variations were categorized into geometrically similar and geometrically comparable weirs. Geometric similarity refers to a condition where all geometric parameters for one labyrinth weir are uniformly scaled to produce a second labyrinth weir. An instance where an arced labyrinth weir has geometrically similar cycles arranged in a similar but not identical configuration is termed 'geometrically comparable' (e.g., weirs with geometrically similar cycles at common or different geometric scales with a different number of cycles). Both of these ideas influenced the scope of arced labyrinth weirs evaluated in this study.

Flow Characteristics

Due to their infinite variability in possible design configurations, arced labyrinth weirs provide unique challenges to designers. Since limited information is available in literature for arced labyrinth weir hydraulics, and few physical models have been tested,

further analysis of their flow characteristics is warranted. These characteristics form the basis of this research.

For example, the characteristic known as 'submergence' occurs when the tailwater elevation exceeds the weir crest elevation; either locally (known as local submergence) or over the entire crest length (Crookston and Tullis 2012c). Nappe interference and aeration (mentioned in Falvey 2003) also lower the discharge efficiency of arced labyrinth weirs. As local submergence increases and flow patterns over the crest change (observed for arced labyrinth weirs), changes in efficiency will also occur. When inlet cycle angle (α') increases (for a given head), instances of local submergence increase and the free-flow capacity of the cycle is maximized. Although weir submergence limits "the gains in discharge efficiency for an arced labyrinth cycle configuration" (Crookston 2010) and local submergence develops sooner for arced labyrinth weirs (compared to non-arced labyrinth weirs), more research is needed on this subject.

Additionally, the literature indicates that the transition of the head-discharge control, in relation to the downstream channel, also affects flow efficiency. For labyrinth weirs in a reservoir application, at higher discharges (higher H_T values), the location of the head-discharge control point can shift from near the weir to a point downstream (Crookston and Tullis 2012a). Essentially, local submergence increases until the entire weir is submerged. Cycle arc angle particularly affects this occurrence (Crookston 2010).

Crookston (2010) tested six arced labyrinth weir geometries (θ = 10°, 20°, 30° for α = 6°, 12°). This study re-evaluated the α = 12° (θ = 10°, 20°) geometries tested by Crookston (2010) and evaluated α = 20° (θ = 0°, 10°, 20°, 30°) labyrinth weirs. α = 20°

approaches the upper limit of nappe stability and aeration potential for labyrinth weirs (Crookston 2010). Crookston suggested that sidewall and cycle arc angle represent significant factors influencing nappe stability, local submergence, and aeration. As a result, parameters such as R, W, and $L_{c\text{-}cycle}$ were the same for each model configuration tested, while α and θ were varied.

Selecting geometry, based on efficiency (as indicated above) and discharge, has also been analyzed by Willmore (2004) using cycle efficiency (ε'). In cases where the spillway footprint, discharge requirements, or construction costs dictate the use of longer weirs, or in contrast, more efficient geometries, cycle efficiency can be used to balance discharge efficiency with cycle length. In fact, when cycle efficiency is used, discharge efficiency is optimized for increased weir lengths. Both Crookston (2010) and Willmore (2004) suggested that cycle efficiency ($\varepsilon' = C_d * L_{c\text{-}cycle}/w$) can be used to represent the effectiveness of the weir and should be examined on arced labyrinth weirs.

Finally, Crookston and Tullis (2012a, b) explored the discharge efficiency of non-arced labyrinth weirs, in reservoir-specific-applications, to see how placement and abutment configurations would affect efficiency. Crookston (2010) investigated six non-arced labyrinth weirs (of $\alpha = 6°$ and 12°) with projecting, flush, and rounded abutment configurations (Fig. 5). These data are compared to arced projecting labyrinth weirs, and for this project, $\alpha = 20°$ sidewall versions of each of those configurations are investigated. Cycle number (mentioned in Crookston and Tullis 2012b) is also explored (using 7 and 10 cycle configurations).

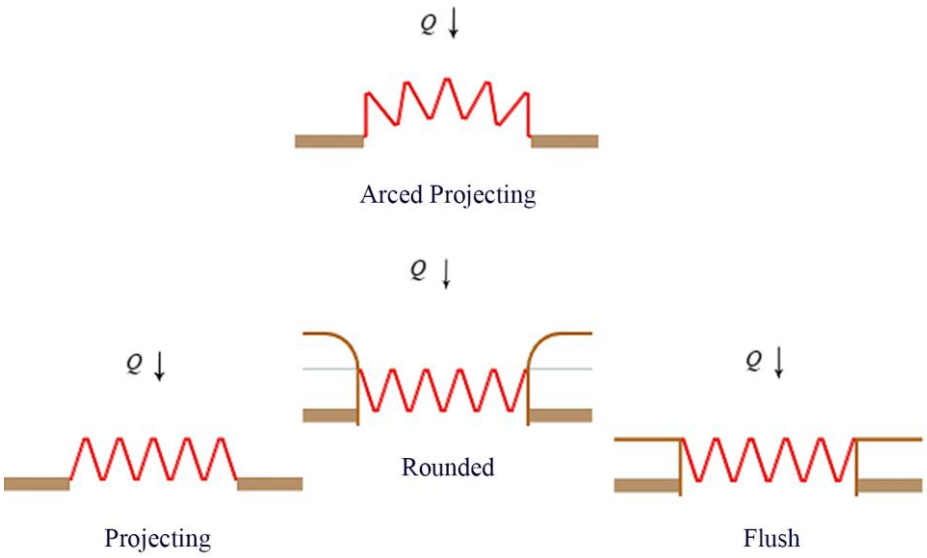

Fig. 5. Weir placement & abutment types.

Research Objectives

This study undertook seven research objectives, which are:

1. Evaluate C_d vs. H_T/P for α = 20° arced labyrinth weirs, with varying cycle arc angles.
2. Explore the effects of geometry, approach flow, nappe aeration, nappe breakers, flow separation, and submergence on arced labyrinth weir discharge efficiency.
3. Evaluate variation in hydraulic performance between geometrically similar and geometrically comparable arced labyrinth weirs with half-round crest shapes.

4. Explore trends in cycle efficiency ($\varepsilon' = C_d * L_{c\text{-}cycle}/w$) suggested by Willmore (2004) and investigated by Crookston (2010) as they relate to arced labyrinth geometries.
5. Evaluate changes in the reservoir approach flow velocity vector fields, with discharge as a function of arced labyrinth weir geometry.
6. Evaluate abutment effects for $\alpha = 20°$ projecting labyrinth weirs.
7. Determine if variations in weir discharge efficiencies exist for geometrically comparable arced labyrinth weirs where N is variable and $L_{c\text{-}cycle}$ and R remain constant.

EXPERIMENTAL SETUP

Test Facilities

Research for this study was performed at the Utah Water Research Laboratory (UWRL) at Utah State University in Logan, UT using an elevated reservoir/headbox facility (Fig. 6). Water was supplied to the reservoir headbox by gravity flow from a reservoir located adjacent to the UWRL via a 20-inch (50.8 cm) supply line or a 6-inch (15.2 cm) supply line for lower discharges (Fig. 7 and 8).

Fig. 6. UWRL & reservoir/headbox.
www.uwrl.usu.edu

The headbox was elevated 4.25 ft (1.3 m) off the ground, by metal beams, to allow supply lines to enter from the bottom. In order to improve approach flow uniformity entering the model reservoir, water was supplied through a diffuser pipe located in a plenum chamber, separated from the model reservoir by a baffle wall. The chamber lined three sides of the headbox (Fig. 9).

Fig. 7. 20-inch (50.8 cm) supply line with mag-meters.

Fig. 8. 6-inch (15.2 cm) supply line with mag-meters.

Fig. 9. Plenum chamber with diffuser pipe and baffled wall.

The headbox was constructed of lumber with steel reinforcement on a steel platform (Fig. A1). Discharge exited the model reservoir via an opening in one sidewall of the headbox. Within the headbox, a level platform was fabricated using a steel-box beam frame supporting a layer of 3/4-inch-thick (~2.0 cm) high-density polyethylene (HDPE) sheeting. The platform measures approximately 14 x 8 ft. (4.26 m x 2.44 m); the test weirs were installed on this level platform. A survey of the apron found it to be level to within ±1/16 inch (1.6 mm).

Labyrinth Weir Model Fabrication and Installation

Eleven models, with 8-inch tall (20 cm) weir walls (P), were fabricated using 1-inch (2.54 cm) thick (t_w) HDPE sheeting. Weir walls were cut from stock material measuring 8 x 4 ft. (2.44 x 1.22 m) in the UWRL shop and planed to ensure uniform thickness. Crookston (2010) found half-round labyrinth weir crest shapes to be

hydraulically more efficient at lower H_T values; therefore, half-round crest shapes were used in this study (Fig. 10). The crest radius (R_{crest}) was equal to half the wall thickness (t_w). The weir walls were assembled with screws and sealed at all joints with NP1® adhesive.

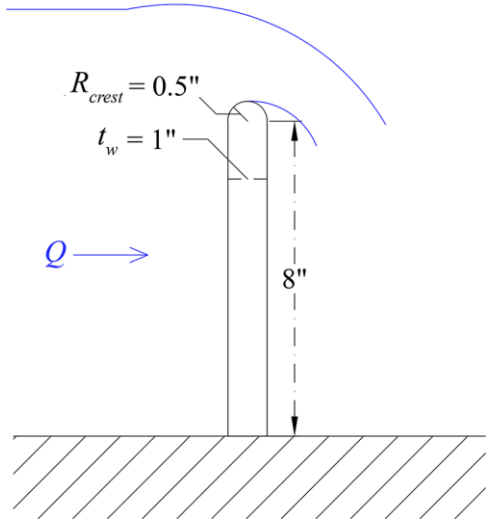

Fig. 10. Half-round crest weir wall.

Labyrinth weir models were secured to the apron using 3-inch (7.62 cm) screws and leveled to within ± 1/64 inch (3.97 mm), as determined by surveying with a Sokkia $B2_0$ automatic level, using shims where needed. The joint between the weir walls and apron was also sealed using NP1® adhesive. Removable headbox/abutment walls were constructed for the various outlet channel widths (W) associated with each model tested (Fig. 11). Layout schematics of all arced and non-arced labyrinth weirs tested are presented in Appendix A.

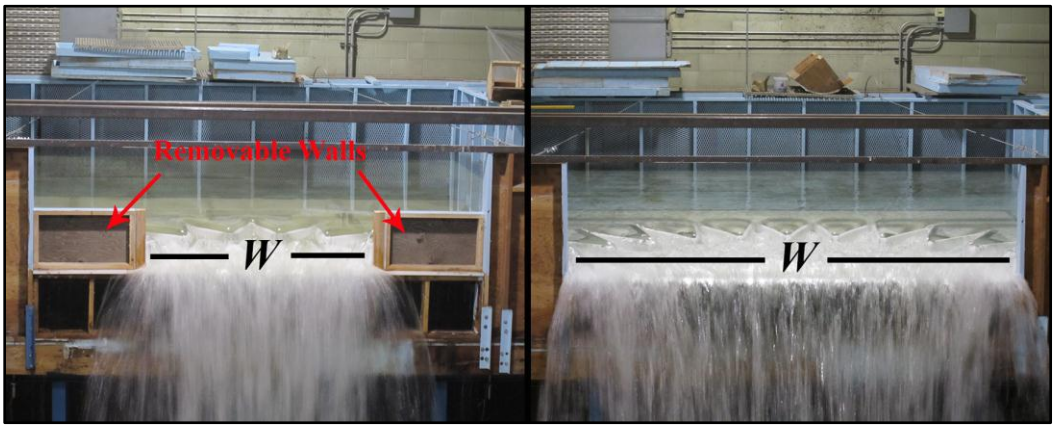

Fig. 11. Removable walls for changing width (W).

Ensuring the levelness of the crest and the crest reference was critical to accurate H_T and ultimately C_d data, particularly at the model scale. To determine the reference crest elevation, a surveying level and rod were used to determine the elevation of 20-30 points distributed along the weir crest; these points were averaged to determine the reference crest elevation and the range of variation from the average noted (Fig. 12). The crest reference elevation was generally within ± 1/32 inch (~0.8 mm). The $B2_0$ level was then rotated, by line of sight, to a survey rod at the stilling basin, and the elevation of the stilling basin invert was determined relative to the weir crest elevation. A point gage inside the stilling basin measured the stilling basin invert; the difference between the weir crest elevation and the stilling basin invert was added to the point gauge reading to determine the crest reference elevation in the stilling well. If more than three points along the crest were found to be outside the range of ± 1/32 inch (~0.8 mm), the weir connection to the apron was tightened or thin metal shims were placed under the weir wall at that point. Complete schematics of the headbox, with a weir installed, are presented in Fig. A1 and A2 of Appendix A.

Fig. 12. Surveying & leveling.

Instrumentation

Two calibrated mag-meters (6- and 20-inch diameter ABB mag-meters®) were used to measure model flow rates with an uncertainty of ± 0.25%. Multi-meters attached to each mag-meter provided meter output frequency (*Hz*) as shown in Fig. 13. The flow meters had been previously calibrated (*Q* vs *Hz*) against a gravimetric flow measurement facility at the UWRL. Leakage in the headbox was accounted for via a leak test where the leak rate was quantified as a function of reservoir depth (typically found to be 0.8% to 3.4% of total flow rate). This was accomplished by filling the headbox to capacity, sealing off the outlet, and using the stilling well to record the stage elevation every 30 minutes. For each model test condition, the corresponding leakage rate was subtracted from the headbox inflow to determine the weir *Q*.

Fig. 13. Multi-meter attached to mag-meter.

Piezometric head was determined by using a stilling basin that connected to a pressure tap in the headbox floor via flexible tubing. The stilling basin pressure tap was located in a relatively undisturbed section of the reservoir where flow velocities were minimal (see Fig. A1). The precision stilling well point gauge (± 0.0005 ft.) measured the water surface elevation (Fig. 14) relative to the weir crest elevation. Due to negligible velocity at the pressure tap location, H_T was assumed to be equal to the piezometric head.

Two-dimensional velocity data were collected on a 1-ft x 1-ft (30.5 x 30.5 cm) grid upstream from each weir at an elevation corresponding to 6/10 of the flow depth, measured down from the surface. These velocity data were measured using a Sontek Flow Tracker 2D probe. Velocity data were logged for approximately 20 to 30 seconds

(Fig. 15) at each point; the X and Y velocity components were then recorded (X corresponding to the direction perpendicular to the outlet channel width). Velocity vector plots were created using MatLab® software (examples are seen in Fig. B1 to B4 of Appendix B). Tracing dye was used to identify streamlines and flow patterns in the reservoir (Fig. 15). Dye was injected with a dye wand placed such that it did not discernibly alter the flow patterns.

Fig. 14. Stilling basin & point gauge.

Fig. 15. Velocity probe & dye wand injection.

TESTING PROCEDURE

Eleven reservoir-specific, half-round crested labyrinth models were tested: eight arced labyrinth weirs and three non-arced labyrinth weirs. A summary schematic is presented in Fig. 16. The test matrix and model dimensions are presented in Table 1. Complete schematics of each labyrinth weir are found in Fig. A3 to A24 of Appendix A.

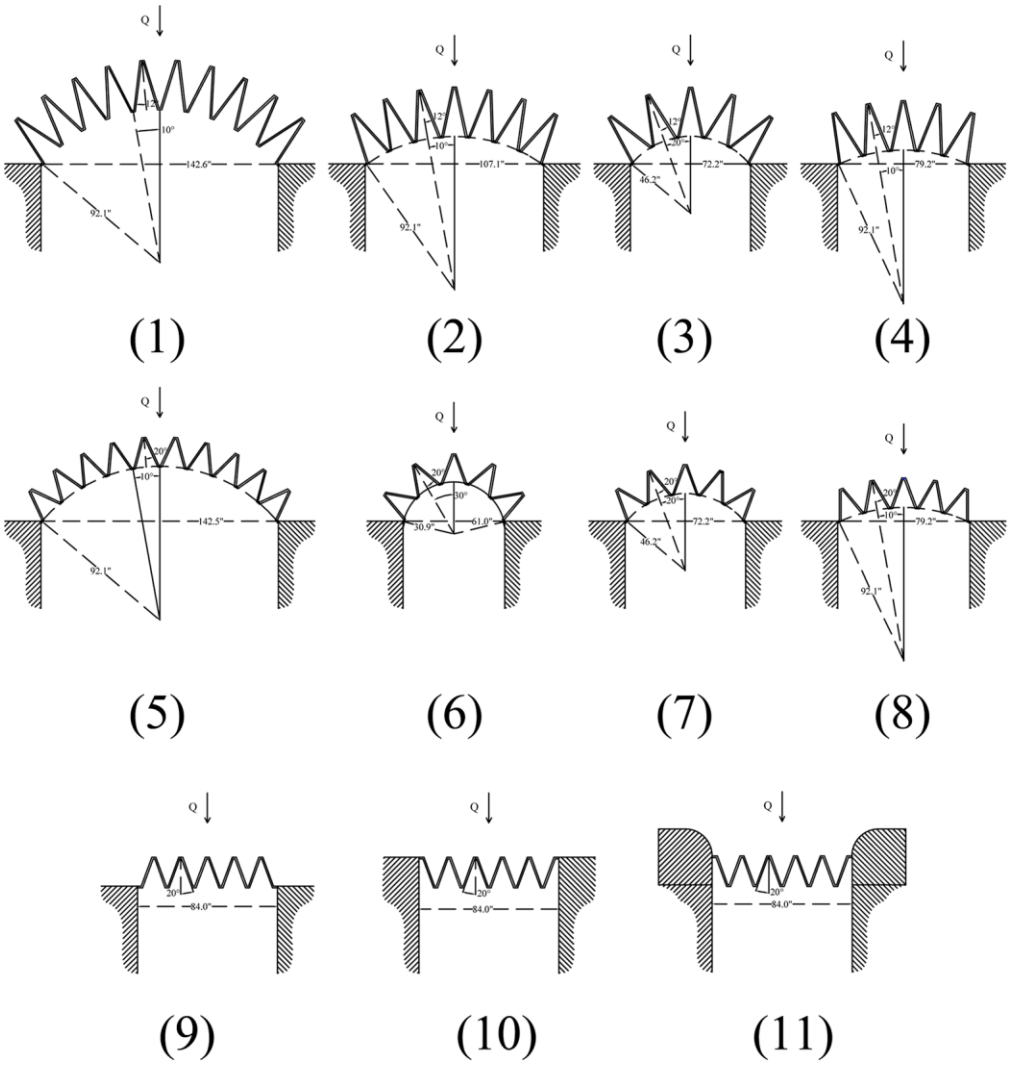

Fig. 16. Summary schematic of models tested.

Table 1. List of models tested in US units.

Model	α	θ	P	$L_{c\text{-}cycle}$	$L_{c\text{-}cycle}/w$	w/P	N	Orientation
1	12	10	8	63.45	3.951	2.008	10	Arced & Projecting
2	12	10	8	63.45	3.951	2.008	7	Arced & Projecting
3	12	20	8	63.45	3.951	2.008	5	Arced & Projecting
4	12	10	8	63.45	3.951	2.008	5	Arced & Projecting
5	20	10	8	40.41	2.516	2.008	10	Arced & Projecting
6	20	30	8	40.41	2.516	2.008	5	Arced & Projecting
7	20	20	8	40.41	2.516	2.008	5	Arced & Projecting
8	20	10	8	40.41	2.516	2.008	5	Arced & Projecting
9	20	0	8	40.41	2.516	2.008	5	Projecting
10	20	0	8	40.41	2.516	2.008	5	Flush
11	20	0	8	40.41	2.516	2.008	5	Rounded Inlet

Thermal expansion/contraction of the HDPE was accounted for by "cooling down" all labyrinth weir models by passing flow over the weirs for 30 minutes prior to collection of head-discharge and weir dimension/elevation reference data [e.g., total crest length (L_c), weir thickness (t_w), weir height (P), and downstream channel width (W)]. Discharge data were collected and averaged over a 7- to 10-minute period once the flow stabilized. Following the flow measurement, point gauge readings were taken (repeated two to three times) to ensure stabilization. These were logged on paper and entered into an excel spreadsheet; nappe conditions were also noted. A single model data set comprised approximately 35 to 50 flow measurements. Data accuracy/repeatability was verified by rechecking data points at every 0.1 H_T/P increment. Flow conditions were documented using digital still and video photography.

The influence of nappe breakers on hydraulic performance was also investigated. Nappe breakers were installed on downstream apexes to artificially aerate the nappe;

hydraulic measurements were taken to determine artificially aerated or vented C_d values. Approximately 10 to 20 data points were collected for each breaker setup. A schematic and photo are shown in Fig. 17.

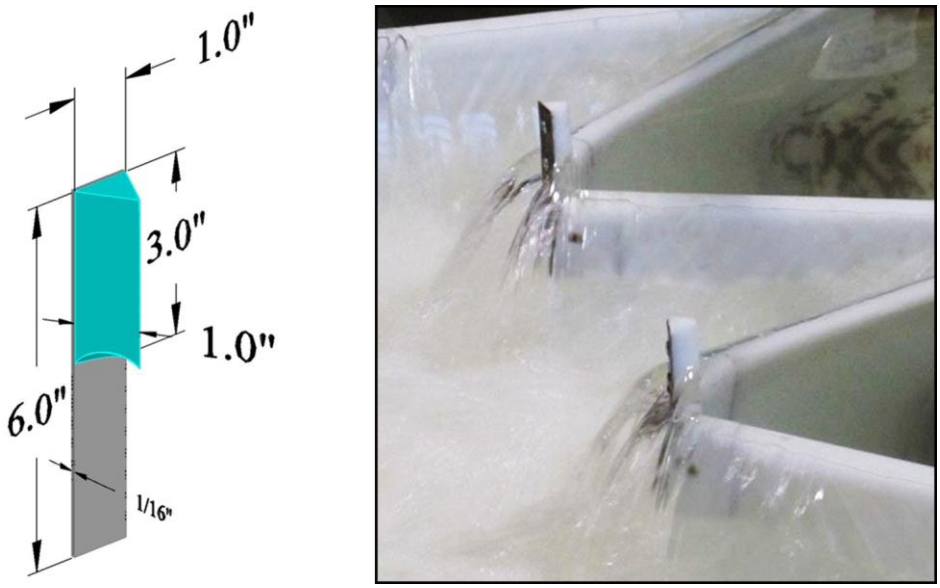

Fig. 17. Nappe breakers.

EXPERIMENTAL RESULTS AND DISCUSSION

C_d (discharge coefficient) data per Eq. [1] were collected from $0.1 \leq H_T/P \leq 0.9$ for 5-cycle configurations and from $0.1 \leq H_T/P \leq 0.5$ for larger cycled weirs. Fig. 18 and 19 show the experimental C_d vs. H_T/P data for α = 12° and 20° sidewall angled weirs, respectively; corresponding tabular data is included in Appendix B. Data curve fits, in the form of Eq. [2], were generated for each weir setup using LAB Fit® with a max error of 1.72%. Eq. [2] represented the best-fit trend line for all model configurations. R^2 values (~0.98 - 0.99) for each curve fit are included in Table 2 along with the coefficients (a, b, c, d). This equation was chosen because of high correlation with the experimental data.

$$C_d = \frac{1}{a\left(\left(\frac{H_T}{P}\right) + b\right)^2 + c} + d \ln\left(\frac{H_T}{P}\right) \qquad [2]$$

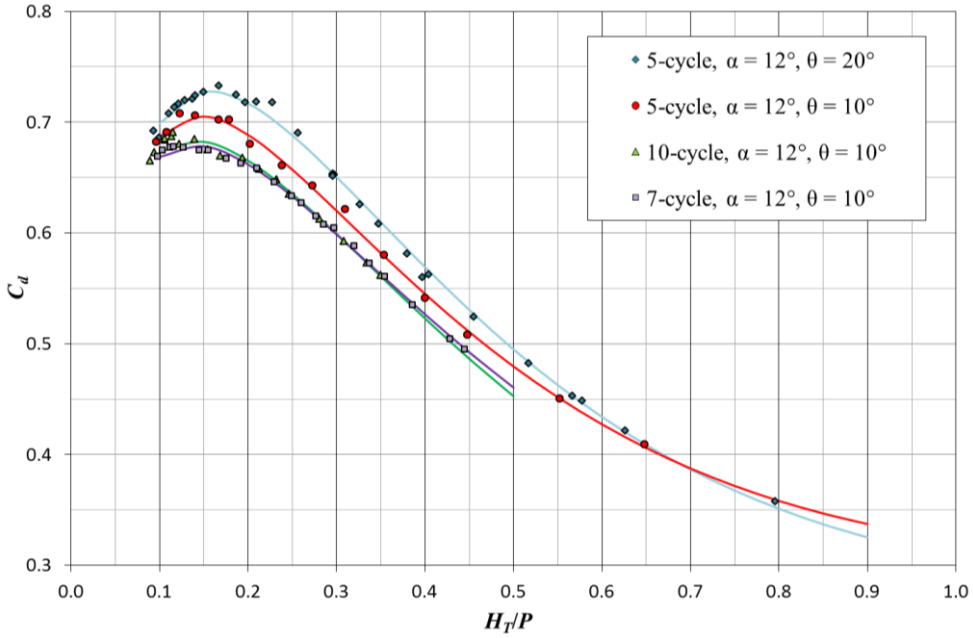

Fig. 18. Sidewall angle α = 12° discharge data with curve fits.

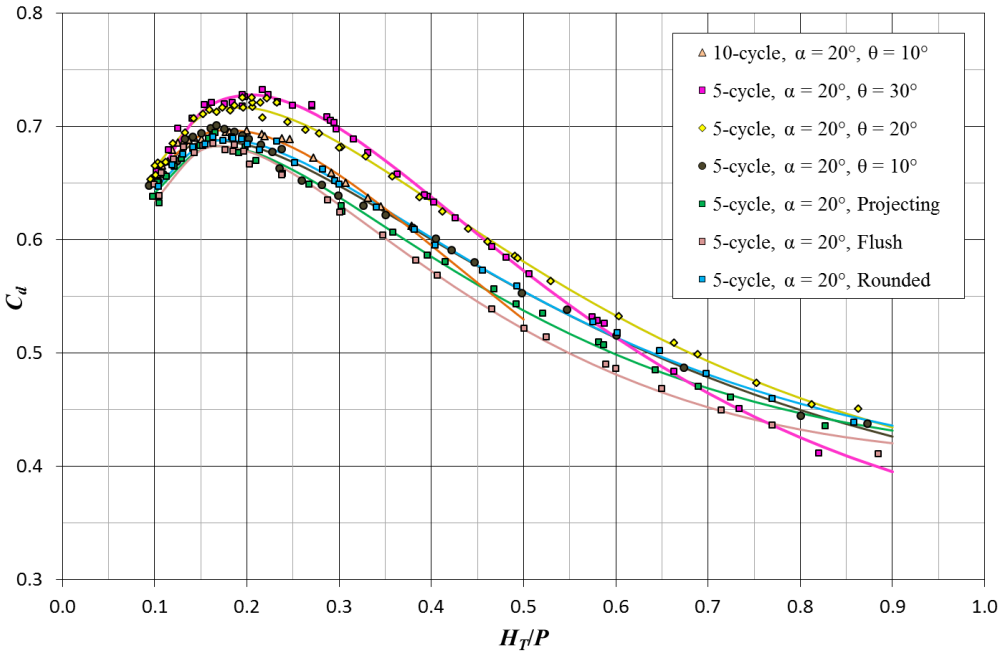

Fig. 19. Sidewall angle α = 20° discharge data with curve fits.

Table 2. Trend line coefficients for half round crests.
Valid for $0.1 \leq H_T/P \leq 0.9$

α (°)		Configuration	Coefficients				R^2 Values
			a	b	c	d	
12	Arced	10cycle, θ = 10°	2.4572	0.1127	0.7944	0.1872	0.9782
		7cycle, θ = 10°	2.1314	0.1591	0.7328	0.2055	0.9956
		* 5cycle, θ = 20°	2.0912	0.1214	0.6269	0.2918	0.9968
		* 5cycle, θ = 10°	1.7196	0.2250	0.5141	0.3258	0.9982
20	Arced	10cycle, θ = 10°	1.9911	0.0794	0.8145	0.2085	0.9948
		5cycle, θ = 30°	1.6622	0.1051	0.6522	0.3178	0.9977
		5cycle, θ = 20°	1.1346	0.2869	0.5312	0.3312	0.9955
		5cycle, θ = 10°	0.8835	0.5070	0.4470	0.2745	0.9852
	Linear	Projecting, θ = 0°	0.9806	0.4446	0.3246	0.4269	0.9938
		Flush	1.1334	0.3550	0.3311	0.4918	0.9907
		Rounded Inlet	0.9642	0.4322	0.3926	0.3724	0.9983

* also tested by Crookston (2010)

Sidewall Angle Effects

Discharge over a weir is directly proportional to the weir length (as per Eq. [1]). When a labyrinth weir is arced, the length is increased for a given channel width, relative to a non-arced labyrinth weir. The allowable weir length for an arced labyrinth weir also increases with decreasing α. Crookston (2010) evaluated arced labyrinth weirs with α = 6° and 12°. This study evaluated some α = 20° arced labyrinth weir geometries, as well as some of the α = 12° geometries evaluated by Crookston (2010).

In this study, nappe aeration behaviors for the α = 12° and 20° arced labyrinth weirs, as illustrated in Fig. 20 and 21, were similar to those noted by Crookston (2010) for in-channel, non-arced labyrinth weirs of the same sidewall angles. The various nappe behaviors are described as clinging, aerated, drowned, partially aerated, unsteady, and unstable (Fig. 22). As water spills over the crest, the nappe behavior is influenced by H_T, crest shape, momentum and trajectory of the flow, turbulence of the headwater, and pressure behind the nappe (Crookston 2010). As H_T increases, aeration conditions normally progress from clinging to aerated (can be unstable for α = 20° weirs) to partially aerated to drowned conditions.

In some cases, specifically with larger values of α, the nappe aeration condition was unsteady (temporal and spatial variations for a given H_T condition). An unsteady nappe may oscillate between clinging and aerated or aerated and drowned. Partial aeration means that the upstream cycle sections feature drowned nappes while the downstream sections of the weir are aerated (i.e., non-uniform). Drowned nappes occur when the momentum of the nappe flow is such that entrained air is carried downstream and not allowed to collect behind the nappe, resulting in a non-aerated nappe condition.

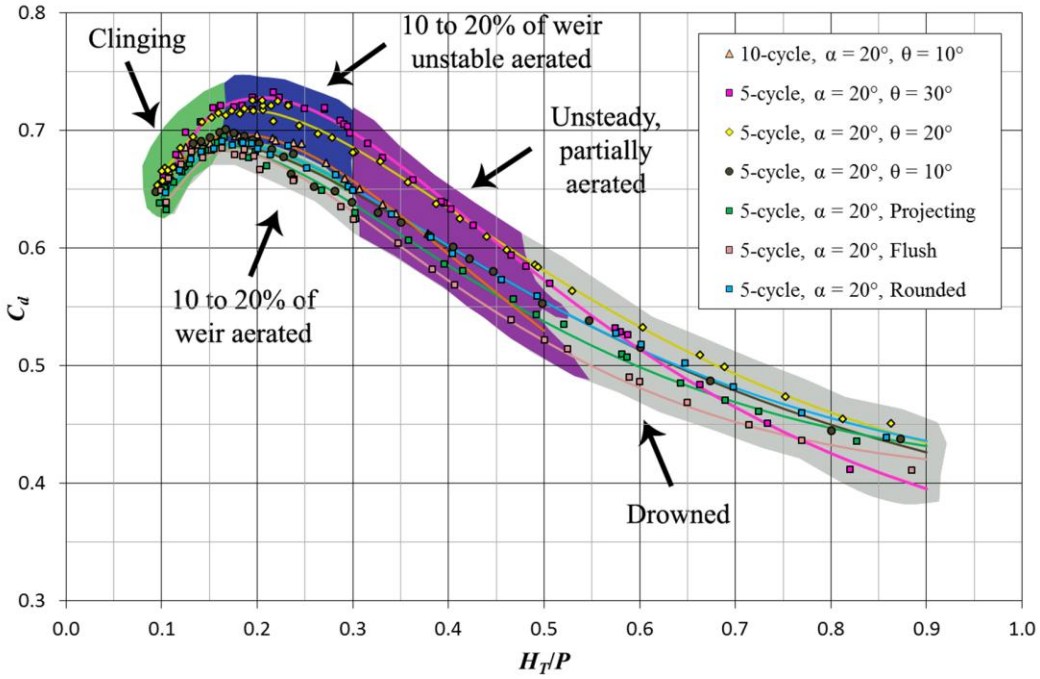

Fig. 20. Nappe aeration conditions for α = 20° sidewall angle.

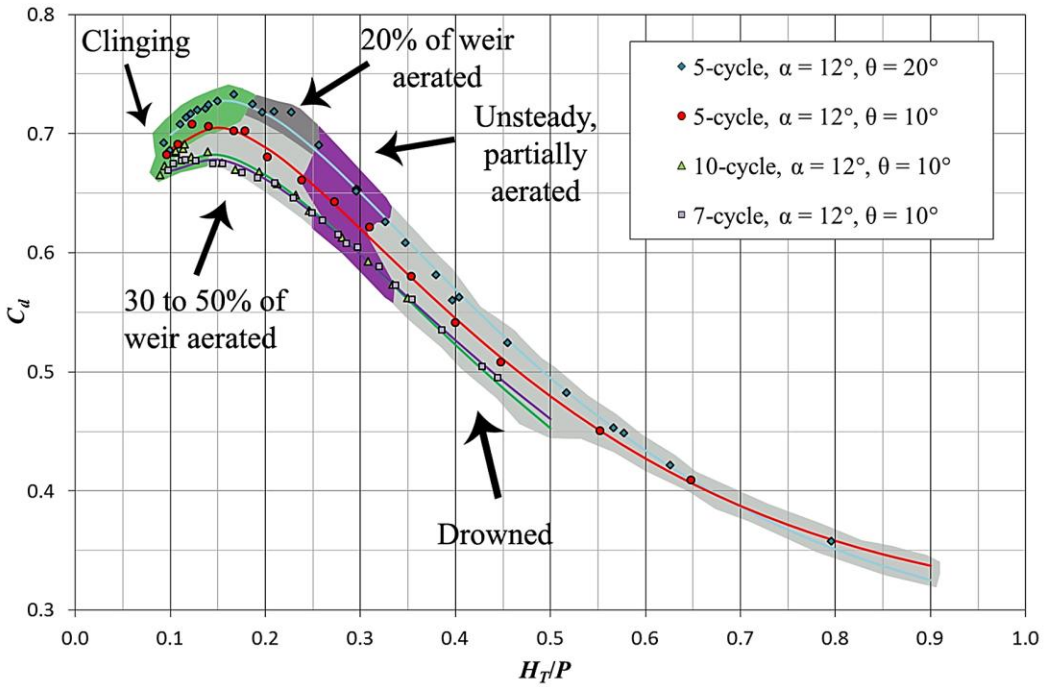

Fig. 21. Nappe aeration conditions for α = 12° sidewall angle.

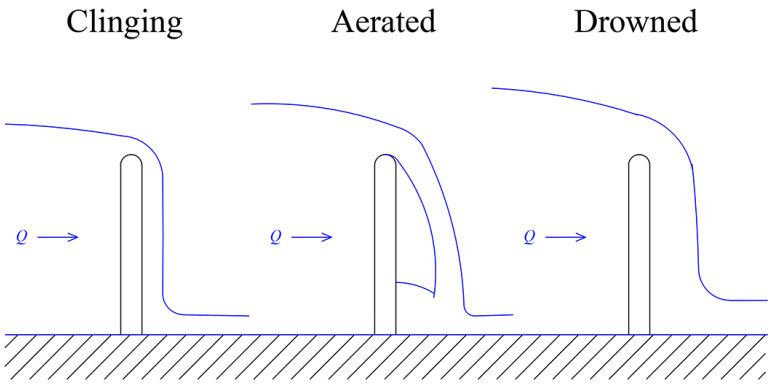

Fig. 22. Half-round aeration conditions and terms.

Nappe instability was observed for α = 20° weirs (θ = 0°, 10°, 20°,30° and N = 5) from 0.18 < H_T/P < 0.3. For prototype structures, this instability may create undesirable noise and pressure fluctuations on the weir structure. Relative to the α = 12° data in Fig. 21, the α = 20° nappes seldom reached full/stable aeration, and if they did, it was only on half-cycles. Figs. 23 and 24 show visual variations in nappe aeration for specific α = 12° and 20° weir configurations (H_T/P = 0.2). All walls of the α = 12° weir (Fig. 23) are naturally aerated; for the α = 20° weir, only the distal sidewalls aerated, while the remaining cycles featured clinging nappes (Fig. 24). Though aerated nappes can be beneficial (e.g., stability of hydrodynamic forces on the weir wall, air entrainment for water quality, etc), naturally aerated nappes are hydraulically less efficient than non-aerated nappes with half-round crests. Although higher sidewall angles are shown to have higher discharges per unit weir width, nappe behavior should also be considered in labyrinth weir design.

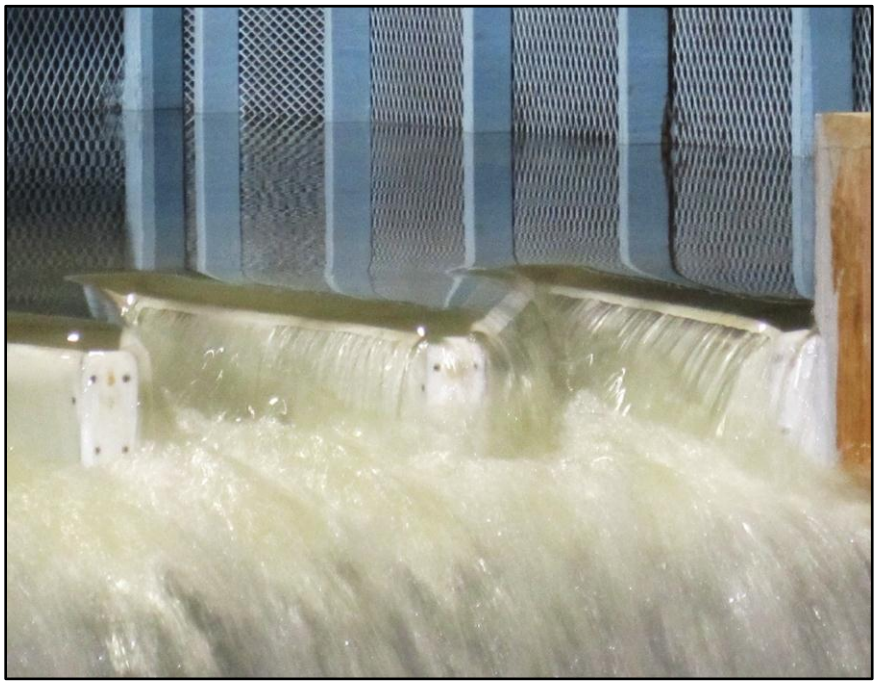

Fig. 23. Natural aeration of 1.5 cycles on α = 12° sidewalls (H_T/P = 0.2).

Fig. 24. Natural aeration of 0.5 cycles on α = 20° sidewalls (H_T/P = 0.2).

Laboratory observations also noted that the drowned nappe condition occurred at lower dimensionless upstream head values for α = 12° weirs (~H_T/P = 0.35) compared to α = 20° weirs (~ H_T/P = 0.5). This is likely due to greater nappe collision and local submergence on smaller sidewall angles, causing the nappe to drown more readily.

Nappe breakers (triangular cross section in plan view) were placed at the downstream apexes of the α = 12° and 20° weirs (θ = 10°, 20° and 30°) tested in this study to investigate their influence on discharge efficiency. Crookston (2010) proposed the downstream apex as an optimal nappe breaker location. C_d data for α = 12° and 20° arced labyrinth weirs with nappe breakers has been normalized by the C_d data of the arced labyrinth weir of the same geometry (α = 12° or 20°) without nappe breakers (natural aeration). These data are presented in Fig. 25 and 26. These nappe breaker data indicate a reduction in discharge efficiency for α = 20° weirs of 5 to 8%. The reduction in discharge efficiency for α = 12° weirs, however, was 3 to 4%. These phenomena appear to be specific to arced labyrinth weirs as Crookston (2010) found no reduction in discharge efficiency when using nappe breakers with traditional (non-arced), in-channel labyrinth weirs.

Nappe breakers vent the nappe to atmospheric pressures, improve stability, and present a potential solution to unstable nappe conditions; however, the decrease in discharge efficiency for arced labyrinth weirs should be accounted for in design. The photograph in Fig. 27 shows the same flow condition and weir configuration as Fig. 24, but with nappe breakers.

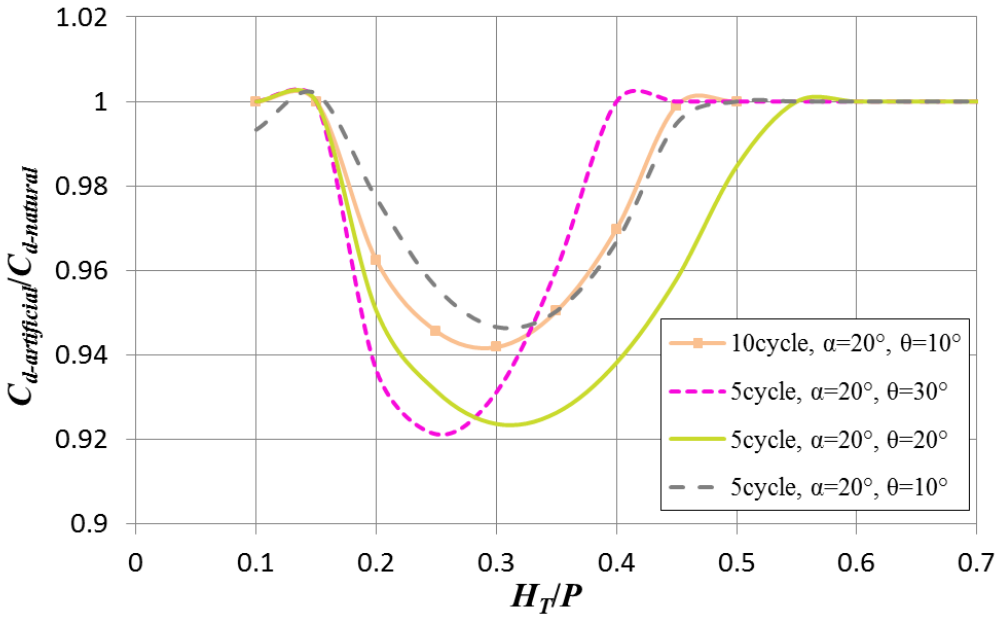

Fig. 25. Artificial nappe aeration C_d data normalized by the natural nappe aeration condition (no nappe breakers) (α = 20°).

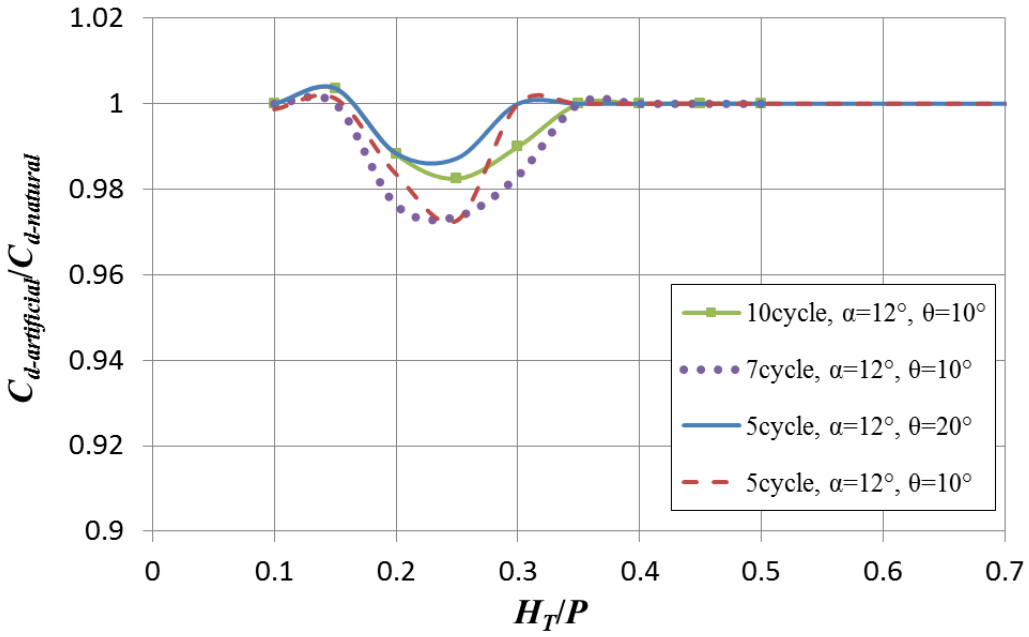

Fig. 26. Artificial nappe aeration C_d data normalized by the natural nappe aeration condition (no nappe breakers) (α = 12°).

Fig. 27. Artificial aeration on α = 20° sidewalls (H_T/P = 0.2) (compare to Fig. 24).

Local submergence is a natural phenomenon observed on arced labyrinth weirs, as well, and partially contributes to a reduction in discharge efficiency. Local submergence occurs sooner (i.e., at lower H_T/P values) for smaller sidewall angles. Since discharge area between sidewalls (at or near upstream apexes) is narrower for α = 12° configurations (from this study) and even narrower for α = 6° weirs (from Crookston 2010), local submergence will cause the local tailwater elevation near the upstream apex to exceed the weir crest elevation and will decrease discharge efficiency locally. Fig. 28 and 29 show a more pronounced local submergence on α = 12° weirs than on α = 20° weirs at the same H_T/P condition due to the reduction in outlet cycle flow area. Although local submergence is expected on arced labyrinth weirs, it does play a role in reduction of discharge.

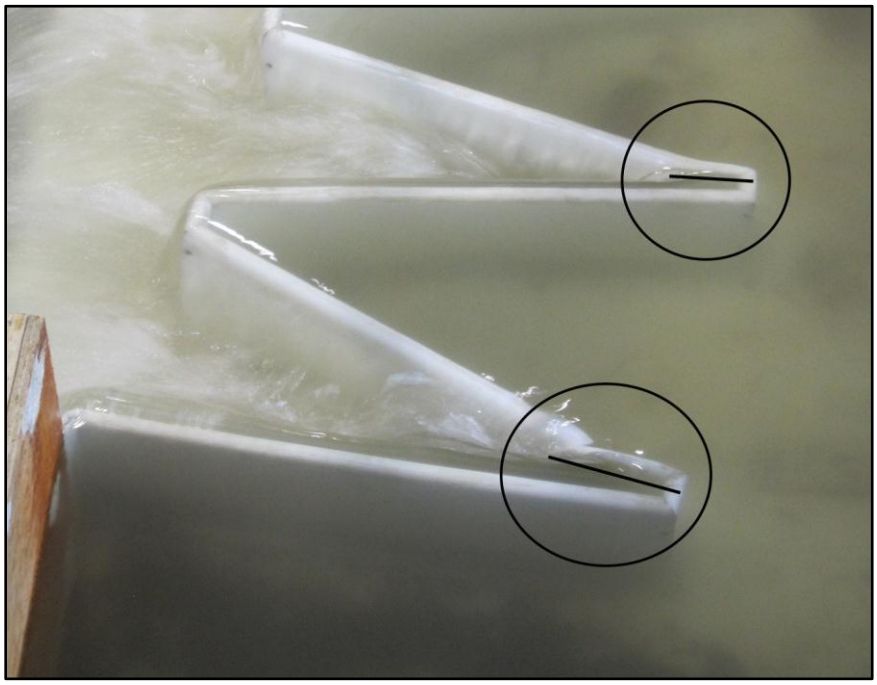

Fig. 28. Local submergence at 0.3 H_T/P on α = 12° sidewall angle.

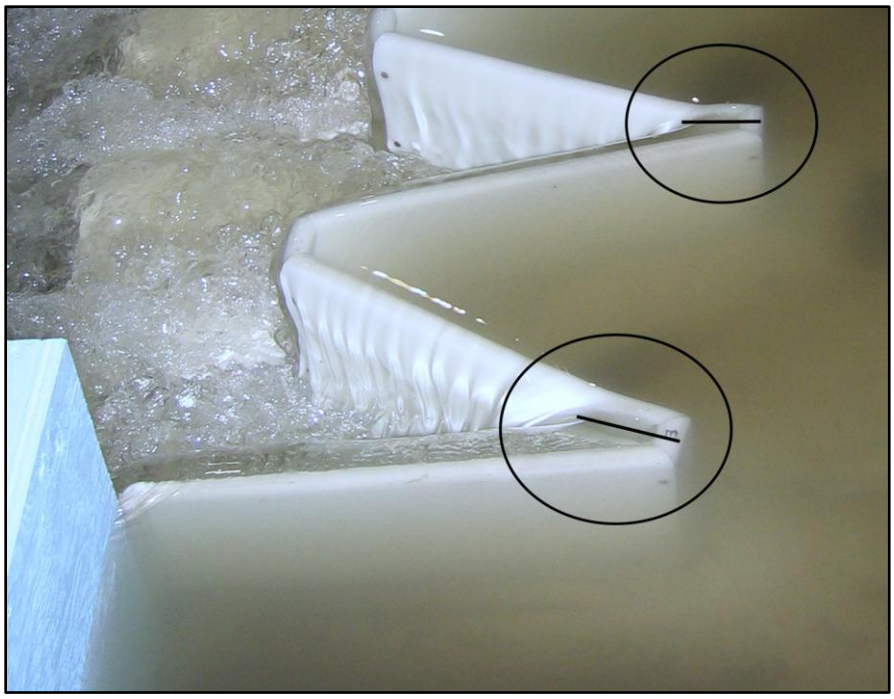

Fig. 29. Local submergence at 0.3 H_T/P on α = 20° sidewall angle.

Crookston (2010) noted that generally, α = 6° arced labyrinth weirs (in-reservoir) are more hydraulically efficient than in-channel labyrinth weirs of the same cycle configuration (see Fig. 30 and 31). The increase in the arced-over-channelized discharge efficiency, however, tends to decrease with increasing α. The maximum increase in discharge efficiency (at low H_T/P values) for the α = 6° (Crookston 2010) and α = 12° (this study) arced labyrinth weirs were approximately 22 - 27% and 4 - 12.5%, respectively. Contrary to that trend, the α = 20° data from the current study was less efficient than the in-channel α = 20° data (see Fig. 32). The α = 20° data in Fig. 32 show reductions in discharge efficiency of the arced labyrinth weir relative to the in-channel labyrinth weir ranging from 0 – 10%.

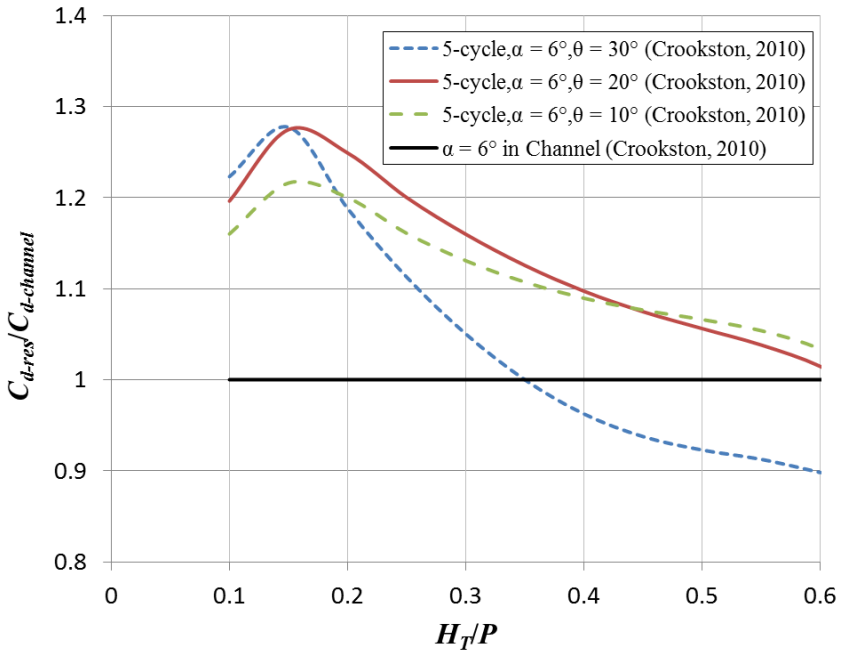

Fig. 30. Arced weir in-reservoir compared to non-arced weir in-channel, α = 6°.

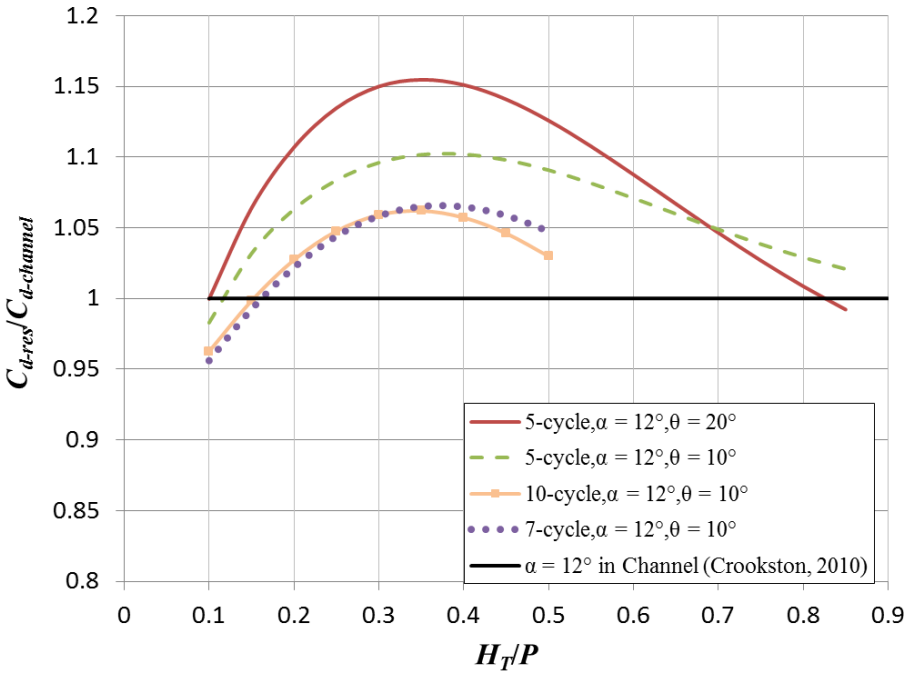

Fig. 31. Arced weir in-reservoir compared to non-arced weir in-channel, α = 12°.

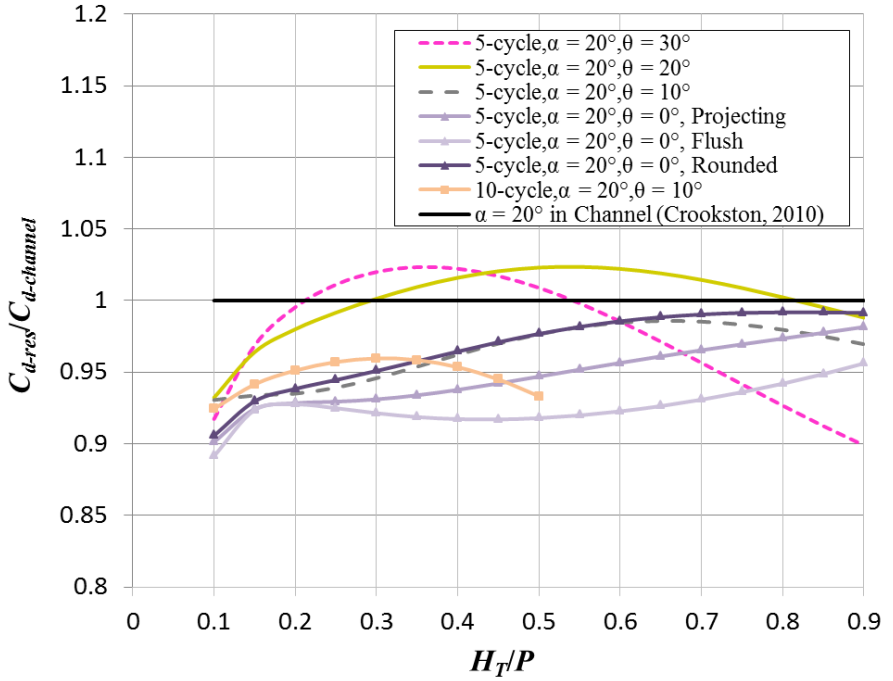

Fig. 32. Arced weir in-reservoir compared to non-arced weir in-channel, α = 20°.

Cycle Efficiency

Willmore (2004) developed 'cycle efficiency' to compare the hydraulic capacity of labyrinth cycles of different α, and L_c but equivalent w. Cycle efficiency (ε') was also discussed by Crookston (2010), and is defined per Eq. [3]. Cycle efficiency represents the discharge per cycle and may be useful in optimizing labyrinth weir designs based on the influence of the following two opposing factors: (1) discharge efficiency (C_d) decreases with decreasing α and (2) $L_{c\text{-cycle}}$ increases with decreasing α (w = constant).

$$\varepsilon' = C_d * \frac{L_{c-cycle}}{w} \qquad [3]$$

In this study, Eq. [3] was plotted versus H_T/P for all weirs tested, and the results are presented in Fig. 33. The data in Fig. 33 indicates that Crookston's α = 6° arced labyrinth weirs were the most efficient per cycle, and α = 20° weirs were the least efficient per cycle. Note that the cycle efficiency (Fig. 33 for example) shows the relative variations in discharge per cycle. The discharge per unit length of weir decreases with decreasing α. In addition to cycle efficiency analyses, economic factors should also be considered.

Cycle Arcing Effects

Variations in the cycle arc angle (θ) and central arc angle (Θ) also affect arced labyrinth weir discharge capacity. θ determines the orientation of individual cycles to the approaching flow. For a given cycle geometry α, increasing θ increases α', resulting in larger inlet cycle flow area. The shape of the arc length θR also approaches a more semicircular shape as θ increases. An important hypothesis throughout the literature

asserts that arced labyrinth weirs are hydraulically more efficient than non-arced weirs in a reservoir. The results of this study support this hypothesis. C_d data for α = 12° and 20° arced labyrinth weirs has been normalized to C_d data for non-arced projecting weirs. These data indicate that for α = 12° and 20° configurations, arcing a labyrinth weir in a reservoir increases discharge efficiency by as much as 10 to 20% (Figs. 34 and 35).

Fig. 34 and 35 also indicate that arced weirs with smaller sidewall angles gain approximately 15% more in discharge efficiency than larger sidewall angles (α = 20°). This may be due to the upstream-downstream cycle flow area ratio (also known as the free-flow capacity of the downstream cycles). This also means that arcing weirs with α = 20° sidewalls will yield less gain in discharge efficiency than arcing weirs with smaller sidewall angles (α < 20°).

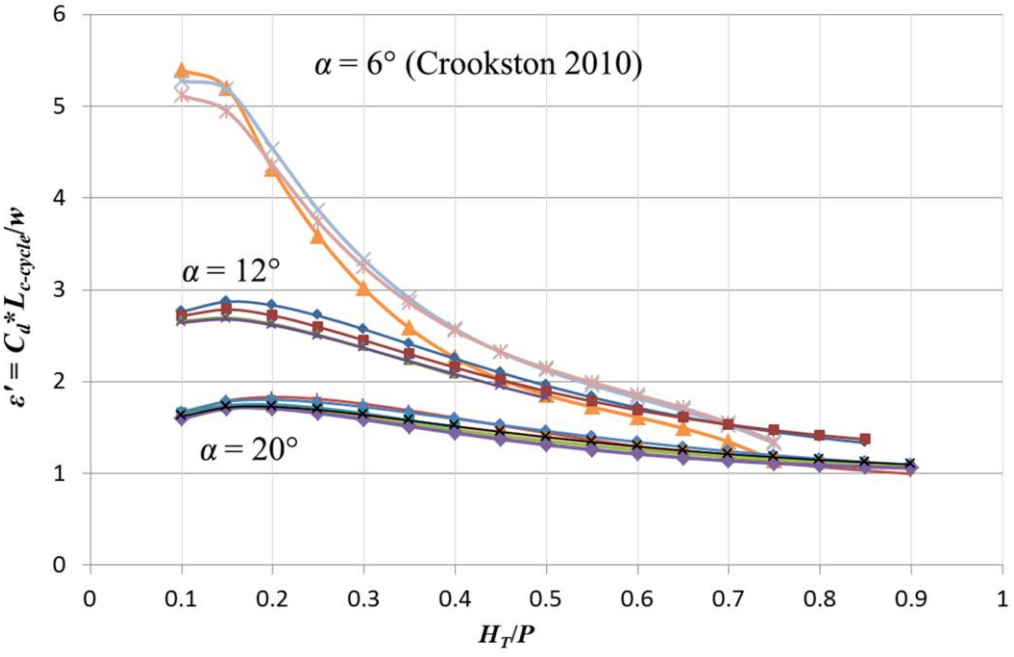

Fig. 33. Cycle efficiency vs. head.

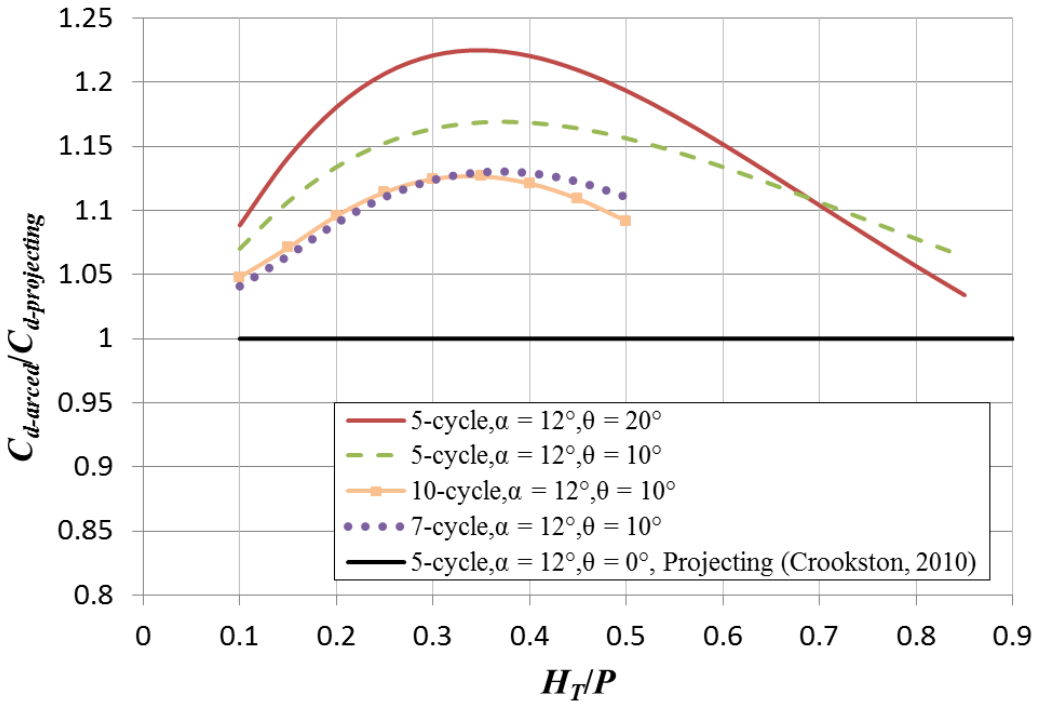

Fig. 34. Arced weir compared to non-arced weir in-reservoir for α = 12°.

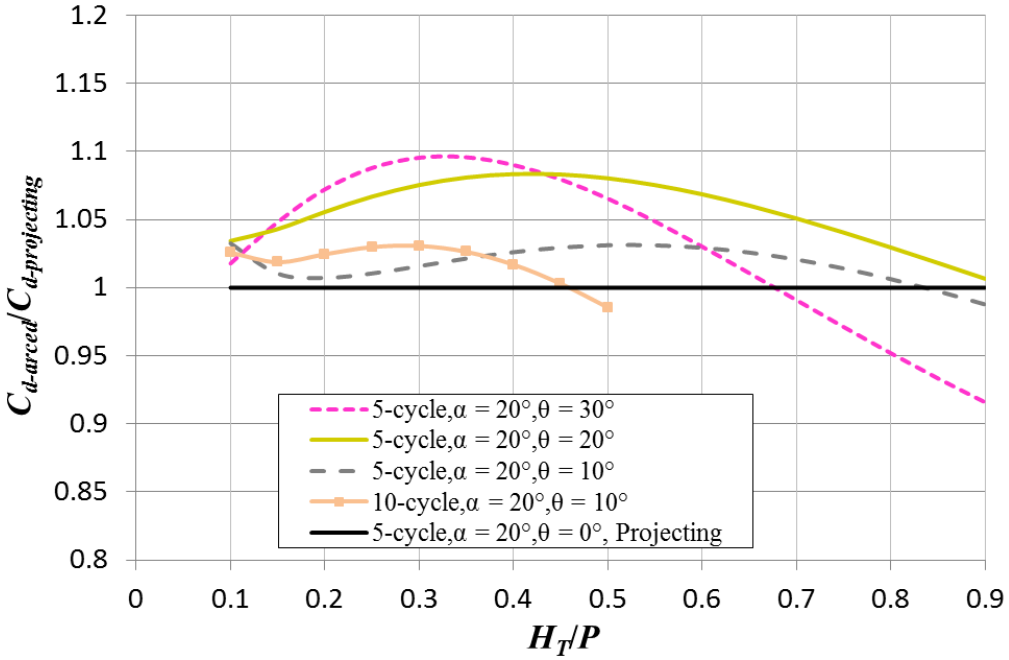

Fig. 35. Arced weir compared to non-arced weir in-reservoir for α = 20°.

Approach Flow Velocity Field

In addition to the increased influence of local submergence as θ and H_T/P increase, the orientation of the streamlines entering an inlet cycle also begin to change from approximately parallel to the cycle centerline to more parallel with the centerline of the outlet channel. Fig. 36 illustrates this shift in approach flow velocity vector orientation for flow conditions corresponding to H_T/P = 0.3 (grey) and 0.6 (black) for a 5-cycle, α = 20°, θ = 30° weir. As this occurs, the arced labyrinth weir begins to act as a form-loss element, adding to the reduction in discharge efficiency. The decline in discharge efficiency (C_d) with increasing H_T/P is more prevalent with increasing θ (see Figs. 34 and 35).

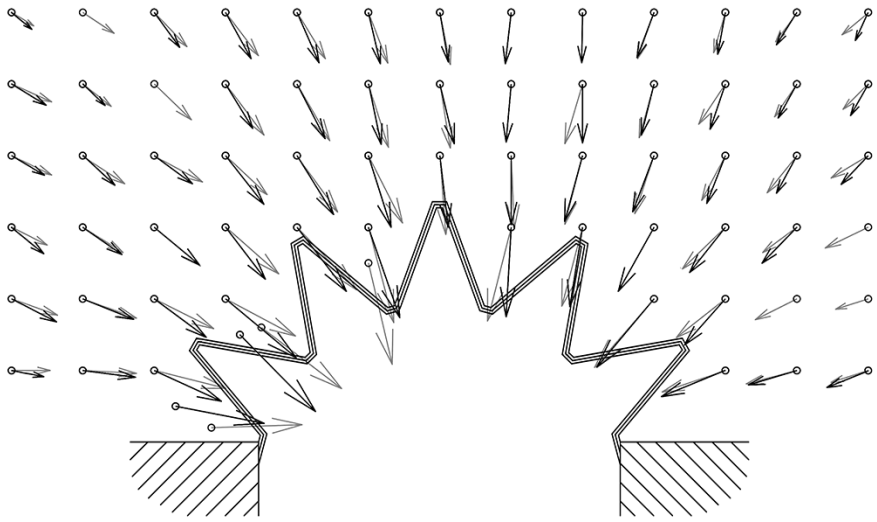

Fig. 36. Head-discharge control point shift, H_T/P = 0.3 (grey) and H_T/P = 0.6 (black).

Arced Labyrinth and Arced Linear Weir Comparison

A shift in the head-discharge control point was seen when comparing discharge on an arced 'linear' weir (Q_{Lin} and arc radius R) to discharge on an arced 'labyrinth' weir (Q_{Lab} and the same R). For linear weirs the head-discharge control point is near the weir crest. By overlaying an arced linear weir on an arced labyrinth weir (at the downstream apexes) the head-discharge control point is comparable (Fig. 37). The percent difference between Q_{Lab} and Q_{Lin} (using C_d data for Q_{Lin}, and a P = 8-inch, t_w = 1-inch, half-round crested arced linear weir) indicates how arced labyrinth weirs (5-cycle, $\alpha = 20°$, $\theta = 30°$) compare to linear weirs ($\alpha = 0°$, $\theta = 0°$) as H_T increases. As percent differences between Q_{Lab} and Q_{Lin} decrease, the head-discharge control point is shifting away from the labyrinth crest to the downstream channel, the weir is submerging, and the arced labyrinth weir is beginning to behave like a linear weir. The data in Table 3 show a decrease in percent difference between Q_{Lab} and Q_{Lin} as H_T/P increases. This decrease indicates a shift in the head-discharge control point to downstream of the weir.

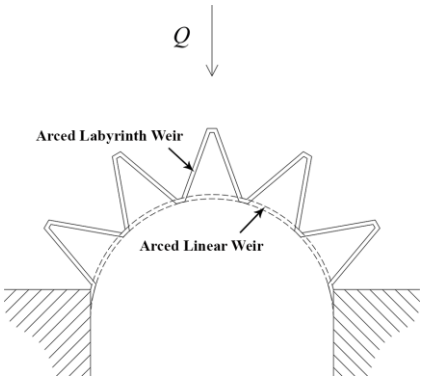

Fig. 37. Arced linear weir (R = 2.58 ft) overlaid on an arced labyrinth weir. (5-cycle, $\alpha = 20°$, R = 2.58 ft)

Table 3. Head-discharge control point shift using Q_{Lab} and Q_{Lin} (notice converging % difference).

H_T/P	Q_{Lab} (cfs)	Q_{Lin} (cfs)	% Difference
0.2	3.11	1.52	68.7
0.3	5.68	3.02	61.1
0.4	7.97	4.48	56.1
0.5	9.49	5.53	52.7
0.6	11.63	7.25	46.5
0.7	13.11	8.74	40.1
0.8	15.3	11.6	27.7

Abutment Effects

The placement of the non-arced labyrinth weirs, either projecting into the reservoir or in the outlet channel, but flush with the reservoir to outlet channel transition, was investigated for an $\alpha = 20°$, $N = 5$ labyrinth weir. Three non-arced labyrinth weir placement types were tested: projecting, flush, and rounded (see Fig. 5 and Appendix A). Crookston did similar testing for $\alpha = 6°$ and 12° non-arced labyrinth weirs (those results are included herein). The rounded and projecting inlet discharge capacities were near equal for the $\alpha = 12°$ weir. For $\alpha = 6°$ the rounded inlet was less efficient than the projecting weir at low heads and again at higher heads. For $\alpha = 20°$ the rounded inlet was 3% more efficient than both the projecting and flush setups (above $H_T/P = 0.2$, Fig. 38). These differences on the $\alpha = 20°$ weir were likely due to natural aeration on the projecting and flush weir cycles.

Compared to the projecting weir (at similar heads, $H_T/P = 0.3$), the rounded inlet prevented unstable nappe formation on inner sidewalls and caused the nappe to remain in a clinging/non-aerated state over a larger range of H_T/P (Fig. 39). For $\alpha = 20°$ weirs, the

rounded inlet also reduced the flow separation and turbulent flow over the crest on distal cycles relative to projecting weirs, allowing for nappe stability and improved discharge efficiency. The flush setup was consistently found to be less efficient for all sidewall angles. Applying these results to arced labyrinth weirs may indicate that rounded inlets can help alleviate instability and flow separation concerns on some arced labyrinth weirs, especially for distal cycles on $\alpha \geq 20°$ weirs.

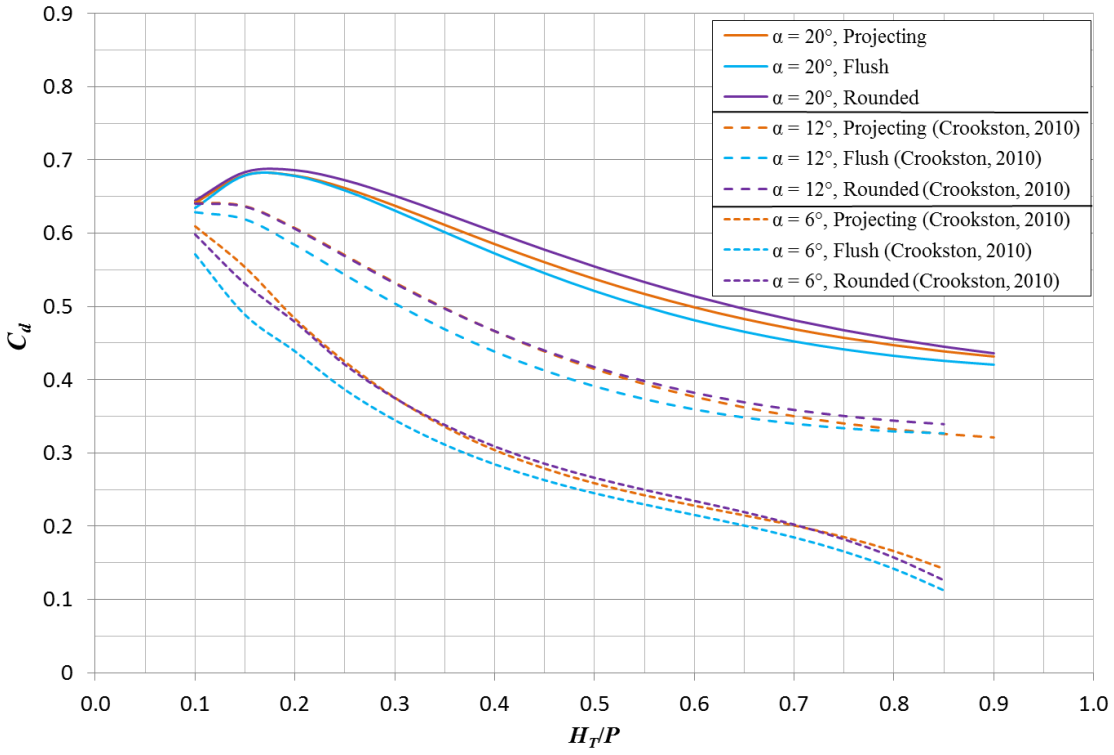

Fig. 38. Comparison of inlet modifications on various sidewall angles.

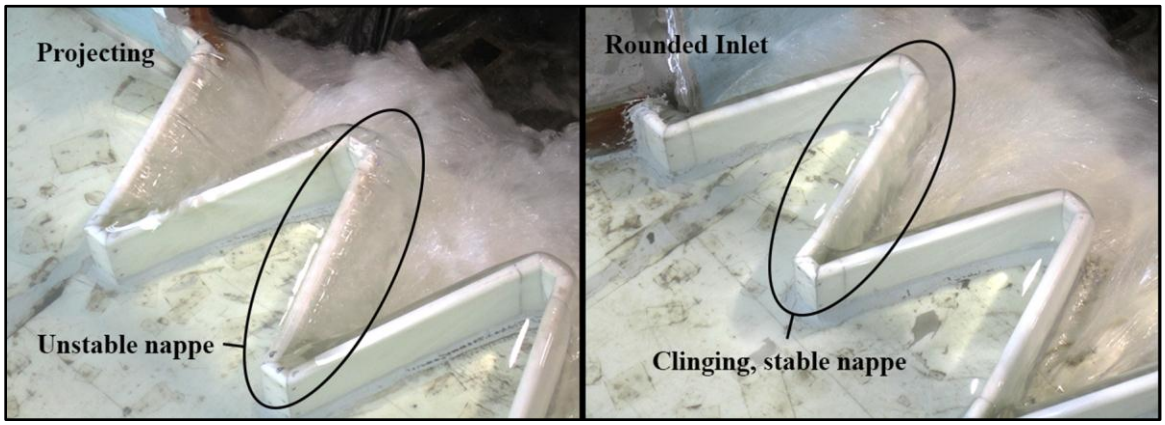

Fig. 39. Projecting weir (Left) vs. rounded inlet weir (Right) at H_T/P = 0.3.

Cycle Number Comparisons

In addition to the arced labyrinth weir models previously discussed, three additional arced labyrinth weirs with differing cycle numbers were tested to determine the influence of N on discharge capacity: a 7-cycle weir (α = 12°) and two 10-cycle weirs (α = 12° and 20°). For α = 12° weirs, the N = 10 and N = 7 configurations were found to be less efficient than N = 5 weirs (above H_T/P = 0.1). For α = 20°, the difference between the discharge coefficients on N = 10 and N = 5 weirs was essentially negligible at the head range tested (Fig. 40).

These results are likely due to nappe aeration conditions and the percent of the weir length aerated. For α = 12° weirs, only 30 to 50% of the 10- and 7-cycle weirs were aerated naturally, while on the 5-cycle weir, 30 to 50% of the crest length was aerated (meaning less weir length was aerated). This likely caused the decrease in efficiency on the larger-cycled weirs. For α = 20° weirs, only 10% of the 10-cycle weir length was aerated and 20% of the 5-cycle weir length was aerated. This makes the difference in the

percentage aerated between the two negligible. More research on discharge efficiency related to cycle number and similar/comparable geometries would be merited.

Since increasing N has a limited effect on C_d values (except with some end effects), the results of this study can be directly applied to arced labyrinth weirs of varying N. It should also be remembered that N does have an effect on discharge capacity as H_T increases (since L_c increases with increasing N). Fig. 41 shows how increased cycle number (or weir length) also increases discharge capacity. Notice that higher discharge capacity exists (at lower heads) for the N = 10 and N = 7 weirs.

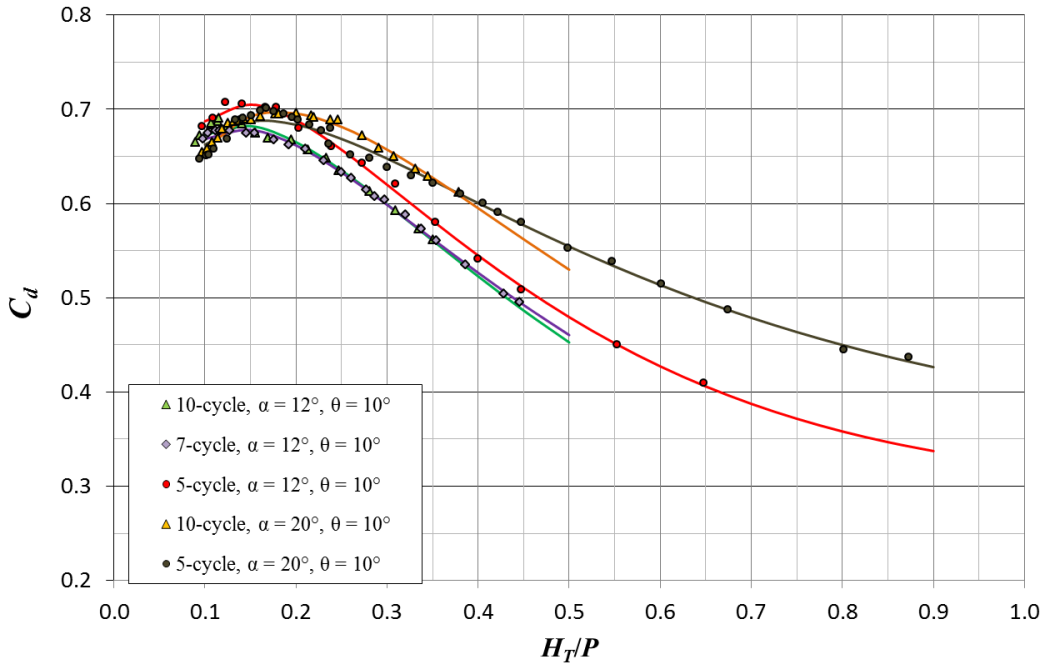

Fig. 40. C_d data for θ = 10° (α = 12° and 20°) weirs with 5, 7, and 10 cycles.

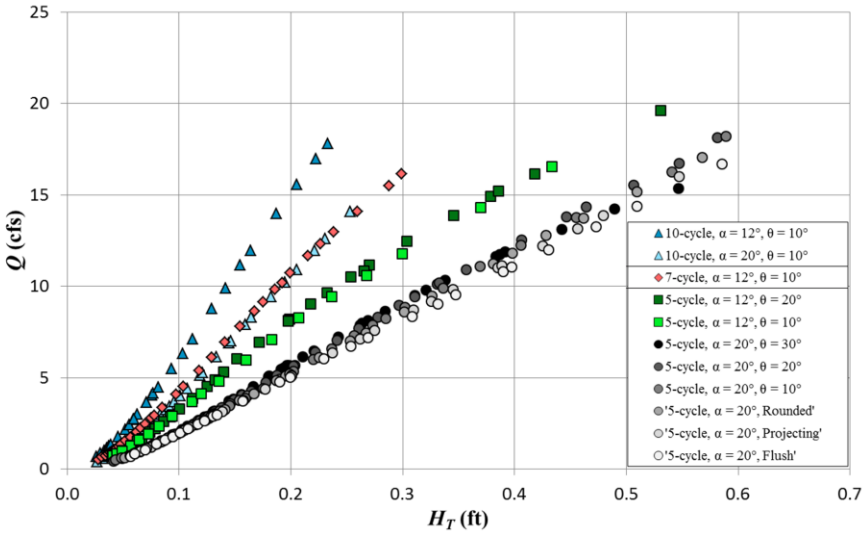

Fig. 41. *Q* vs. H_T (*N* emphasized) for all models.

Sources of Error & Uncertainty

Applying the techniques described in Kline and McClintock (1953) for single sample experiments, the percent uncertainty and error for this study were calculated at each data point. A partial derivative, for physical measurements, was quantified within the uncertainty interval at each flow rate. The error ranges for physical measurements were:

$$\omega_Q = \pm 0.25\%$$

$$\omega_{Lc} = \pm 1/64 \text{ in}$$

$$\omega_P = \pm 0.0005 \text{ ft}$$

$$\omega_W = \pm 1/32 \text{ in}$$

$$\omega_{HT} = \pm 0.0005 \text{ ft}$$

A VBA code, seen in Appendix C, was then used to calculate uncertainty at each data point. The tabular uncertainty data are found in Appendix B. The average percent uncertainty for the entire data set was found to be 1.75% ± 0.011 C_d. The maximum percent uncertainty occurred on the weir model with the longest crest length (10-cycle, α = 20°, θ = 10°); it was found to be 8.74% ± 0.02 C_d. This low uncertainty indicates very reliable experimental results and procedures. The complete range of uncertainty across all models was found to be 0.70% to 8.74%.

The sources of error in this experiment included difficulty in leveling longer crest lengths, measurement inaccuracies on longer crest lengths, low precision of mag-meter flow rates at low heads, apron warping under extended use, headbox leakage and warping after extended use, sediment interference with point gage readings, and human error.

The most probable source of error, however, was a slight discrepancy in crest reference measurement between Crookston's (2010) data and the data in this project. The α = 12° data (from Crookston 2010) used in this report, contains a lower (unpublished) crest reference not seen in the original Crookston (2010) manuscript (lowering the data slightly). Two exact weirs, originally tested by Crookston (2010), were also tested herein to verify the use of the unpublished crest reference (with approval). All trends and conclusions between this project and Crookston's (2010) project still correlate well.

APPLICATION OF RESULTS

The results of this study can point engineers to an ideal geometry for arced labyrinth weir prototypes. They also identify important hydraulic issues that may arise on installed weirs (keeping in mind the scope and scale of the information presented herein). Although no design method is presented aeration data (Figs. 20 and 21) and Q vs. H_T data (Figs. 41 to 43) for arced labyrinth weirs are given to help select optimal geometries. Together with Crookston (2010) data, Fig. 41 to 43 provide means for matching hydraulic requirements of an actual system to flows tested in the laboratory.

In Fig. 41 (seen in the previous section), the Q vs. H_T graph shows how N affects discharge. In Figs. 42 and 43, the graphs are changed to emphasize α and θ (and to include Crookston 2010 data). Froude scaling techniques (ASCE 2000) could then be used to predict prototype discharge (of an actual system) based upon these flow rates.

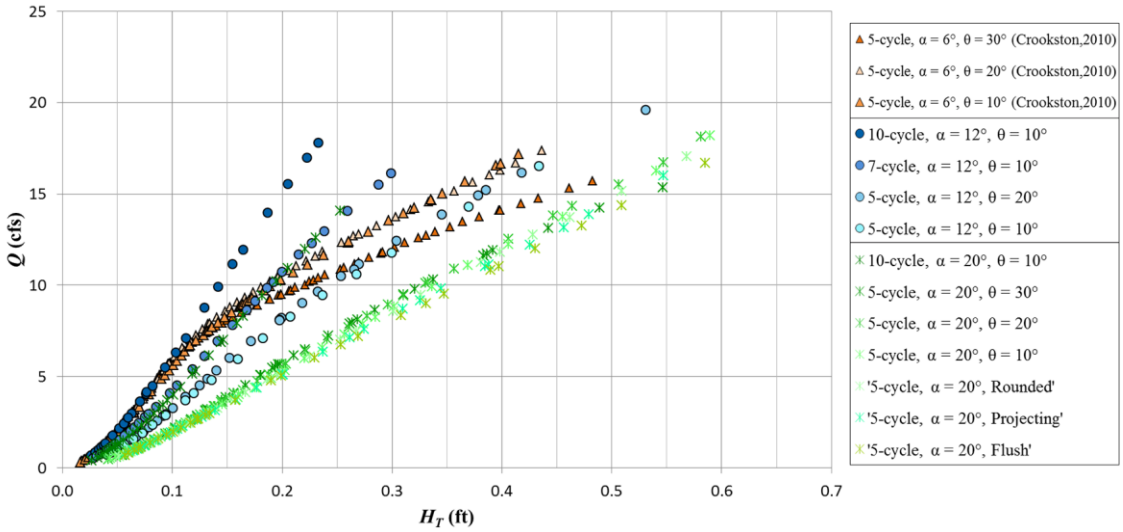

Fig. 42. Q vs. H_T (α emphasized) for all models.

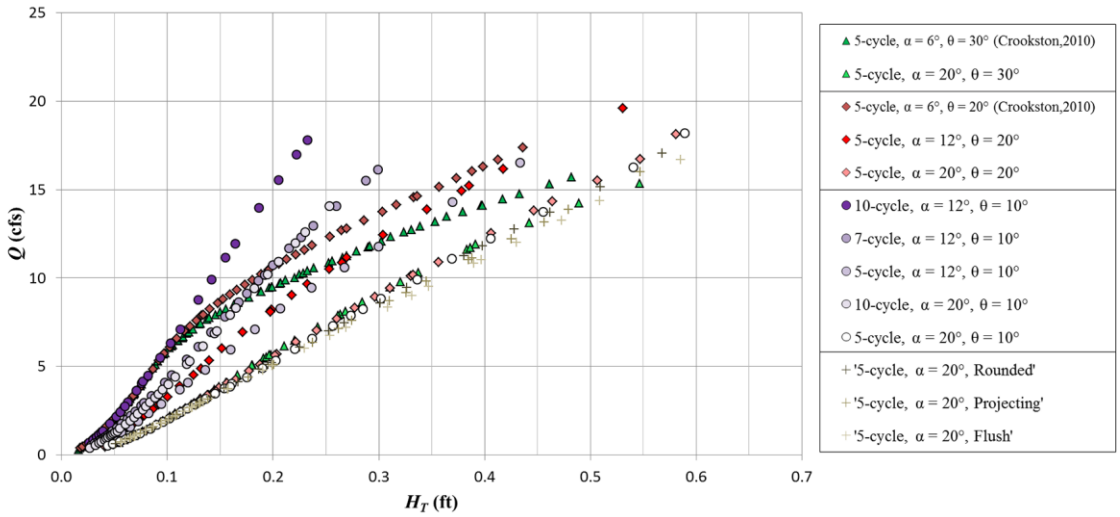

Fig. 43. Q vs. H_T (θ emphasized) for all models.

Sound engineering judgement should be used to balance discharge capacity with weir discharge efficiency. If the most efficient weir is desired, then C_d data from Fig. 18 and 19 could be used (note that C_d data can also be used to predict Q) in conjunction with ε' data. However, both capacity and efficiency data should be scaled appropriately if and only if the limitations of the laboratory-scale models are understood.

CONCLUSIONS & RECOMMENDATIONS

The objective of this study was to develop an increased understanding of the hydraulic characteristics of arced labyrinth weirs. Arced labyrinth weirs are complex hydraulic structures that generate 3-dimensional flow patterns and feature additional geometric parameters, relative to non-arced labyrinth weirs, that can influence discharge efficiency. Based on the results presented, the following conclusions are made:

1. Consistent with non-arced, channelized labyrinth weirs, the discharge efficiency (as quantified by C_d) decreases with decreasing sidewall angle (α). This phenomenon is due, in part, to the increased influence of local submergence, natural aeration potential of the nappe, and relative offset between the weir sidewall and flow vectors as H_T/P increases.
2. For larger sidewall angles ($\alpha \geq 20°$), nappe instabilities exist at H_T/P values from 0.15 to 0.3. These nappe instability problems were alleviated by use of nappe breakers on downstream apexes (which also lowered discharge efficiency) or rounded abutment modifications.
3. A cycle efficiency (ε') analysis showed that, for the arced labyrinth weir geometries considered, the discharge per cycle increased with decreasing sidewall angle [i.e., the effects of decreasing C_d with decreasing α more than compensated for the increase in weir length (for a channel of constant width) with decreasing α]. Note that cycle efficiency is based solely on discharge capacity; an economic analysis of alternative design options should also be considered.

4. Increasing cycle arc angle (θ) increases the flow area in the inlet cycles, and better orients the inlet cycles to the reservoir approach flow, resulting in increased discharge capacity. The discharge efficiency gains are lost, however, at higher H_T/P values (≥ 0.4) as the approach flow vector orientation changes from an inlet cycle alignment to a downstream channel alignment.
5. Abutment wall detail influences the hydraulic efficiency of projecting labyrinth weirs (reservoir applications). For $\alpha = 20°$ weirs the rounded inlet proved to be the most efficient modification tested, but these gains were negligible and decreased as α decreased.
6. Finally, if similar cycles are used, cycle number (N) was found to have only a modest effect, if any, on weir discharge efficiency. For smaller sidewall angles, it caused a slightly greater percent of aeration, but the effect on efficiency was minimal. In contrast, higher cycle number increased weir length and discharge capacity for a given H_T.

Future arced labyrinth weir research should include evaluating other crest shapes, sidewall angles and determining the influence (in a general sense) of upstream reservoir topographies that differ from the horizontal aprons tested herein, and investigating the influence of abutments on arced configurations.

REFERENCES

ASCE. (2000). "Hydraulic modeling: Concepts and practice." Manual 97, ASCE, Reston, Va.

Copeland, R. R., and Fletcher, B. P. (2000). "Model study of Prado Spillway." U.S. Army Corps of Engineers, Research and Development Center, ERDC/CHL TR-00-17. 16-17 p.

Cordero Page, D., Elviro Garcia, V., and Granell Ninot, C. (2007). "Aliviaderos en laberinto. Presa de Maria Cristina." *Ingenieria Civil* 146:15-18. (Spanish).

Crookston, B. (2010). "Labyrinth weirs." PhD dissertation. Utah State University Library, Logan, Utah. 44-66, 95-122 p.

Crookston, B., and Tullis, B. (2012a). "Arced labyrinth weirs." *J. Hydraul. Eng.*, ASCE, 137(6): 555-562.

Crookston, B., and Tullis, B. (2012b). "Discharge efficiency of reservoir-application-specific labyrinth weirs." *J. Irrig. and Drain. Eng.*, Technical Note, ASCE, 138(6): 564-568.

Crookston, B., and Tullis, B. (2012c). "Labyrinth weirs: nappe interference and local submergence." *J. Irrig. and Drain. Eng.*, ASCE, 138(8): 757-765.

Darvas, L. (1971). "Discussion of performance and design of labyrinth weirs, by Hay and Taylor." *J. Hydraul. Eng.*, ASCE, 97(80), 1246-1251.

Falvey, H. (2003). *Hydraulic design of labyrinth weirs.* ASCE Press, Reston, Va.

Gentilini, B. (1940). "Stramazzi con cresta a planta obliqua e a zig-zag." Memorie e Studi dell Instituto di Idraulica e Construzioni Idrauliche del Regil Politecnico di Milano, No. 48 (in Italian).

Hay, N., and Taylor, G. (1970). "Performance and design of labyrinth weirs." *J. Hydraul. Eng.*, ASCE, 96(11), 2337-2357.

Henderson, F. (1966). "Channel controls." *Open channel flow*. MacMillan, New York, 174-176.

Hinchliff, D., and Houston, K. (1984). "Hydraulic design and application of labyrinth spillways." *Proc. of 4th Annu. USCOLD Lecture.*

Houston, K. (1982). "Hydraulic model study of Ute Dam labyrinth spillway." US Bureau of Reclamations, Denver, Colo., # GR 82-13, 41 p.

Houston, K. (1983). "Hydraulic model study of Hyrum Dam auxiliary labyrinth spillway." U.S. Bureau of Reclamations, Denver, Colo., # GR 82-13, 9-10 p.

Kline S. J., and McClintock, F. A. (1953). "Describing uncertainties in single-sample experiments." *Mech. Eng.* 75(1): 3-8.

Kocahan, H., and Taylor, G. (2002). *Rehabilitation of Black Rock Dam "seepage & inadequate spillway."* Hydroplus, Inc., Arlington, Va.

Lopes, R., Matos, J., and Melo, J. (2008). "Characteristic depths and energy dissipation downstream of a labyrinth weir." *Proc. of the Int. Junior Researcher. and Eng. Workshop on Hydraul. Structures (IJREWHS '08)*, Pisa, Italy.

Lux, F. (1984). "Discharge characteristics of labyrinth weirs." *Proc. of Conf. on Water for Resources Dev.*, ASCE, Cour d'Alene, Idaho.

Magalhaes, P. (1985). "Labyrinth-weir spillways." *Proc. of 15th Annu. ICOLD*, Vol IV, Lausanne, Switzerland, p. 395-407.

Savage, B., Frizell, K., and Crowder, J. (2004). "Brain versus brawn: The changing world of hydraulic model studies." *Proc. of the ASDSO Annu. Conf.*, Phoenix, Ariz., CD-ROM.

Tacail, F. G., Evans, B., and Bibb, A. (1990). "Case study of a labyrinth weir spillway." *Canadian J. Civ. Eng.*, 17(1):1-7.

Taylor, G. (1968). "The performance of labyrinth weirs." PhD thesis, University of Nottingham, Nottingham, UK.

Tullis, B., and Young, J. (2005). "Lake Brazos Dam model study of the existing spillway structure and a new labyrinth weir spillway structure." Hydraul. Report No. 1575, Utah Water Research Laboratory, Logan, Utah.

Tullis, B., Young, J., and Chandler, M. (2007). "Head-discharge relationships for submerged labyrinth weirs." *J. Hydraul. Eng.*, ASCE, 133(3): 248-254.

Tullis, J. P. (1992). "Weatherford spillway model study." Hydraul. Report No. 3011, Utah Water Research Laboratory, Logan, Utah.

Tullis, J. P., Nosratollah, H., and Waldron, D. (1995). "Design of labyrinth spillways." *J. Hydraul. Eng.*, ASCE, 121(3): 247-255.

Willmore, C. (2004). "Hydraulic characteristics of labyrinth weirs." MS report, Utah State University Library, Logan, Utah.

Wilson, S. (1995). "Weatherford supply reservoir radial labyrinth spillway." *Water Resources Eng.*, ASCE, Reston, Va.

Yildiz, D. and Uzecek, E. (1996). "Modeling the performance of labyrinth spillways." *Hydropower & Dams*. Aqua-Media Int. Ltd., Surrey, UK. 3:71-76.

APPENDICES

APPENDIX A

Drawings & Photographs

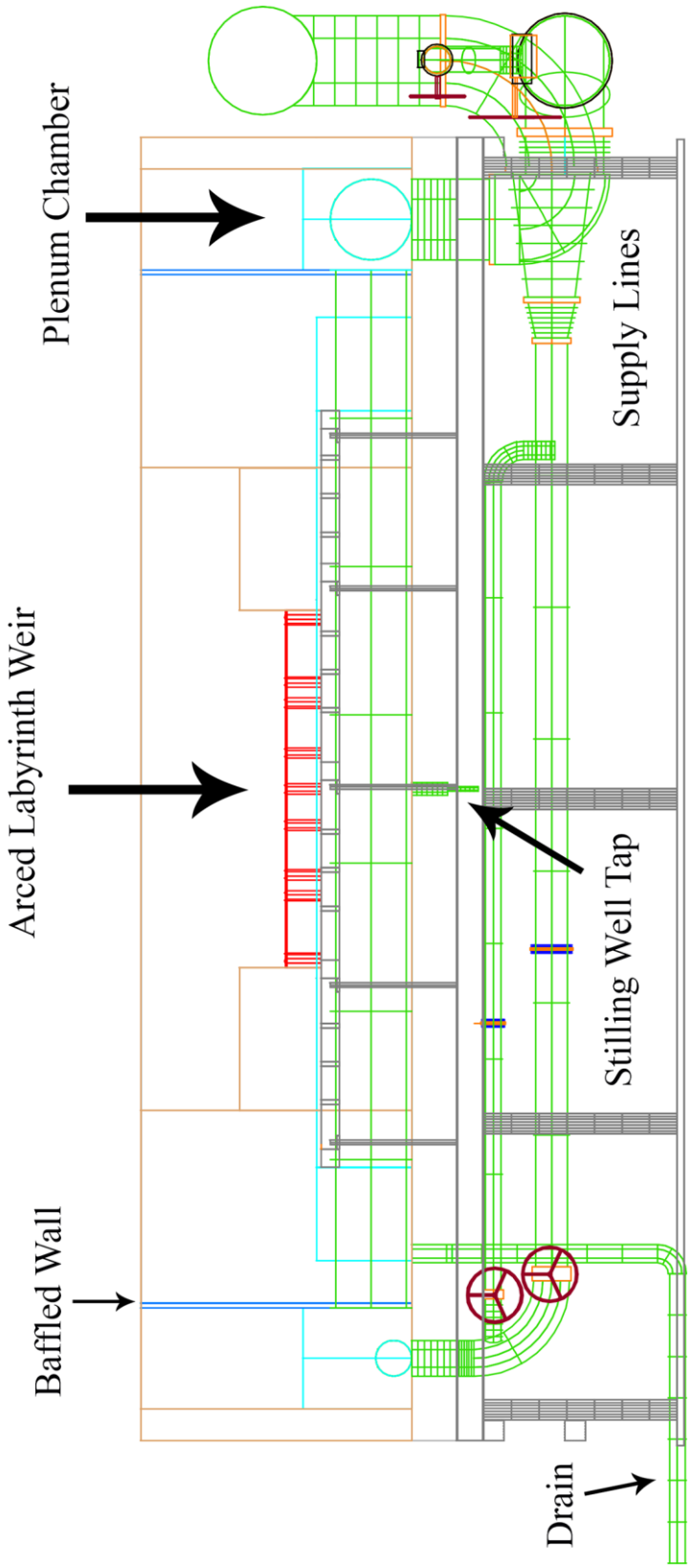

Fig. A1. Headbox 2D elevation schematic.

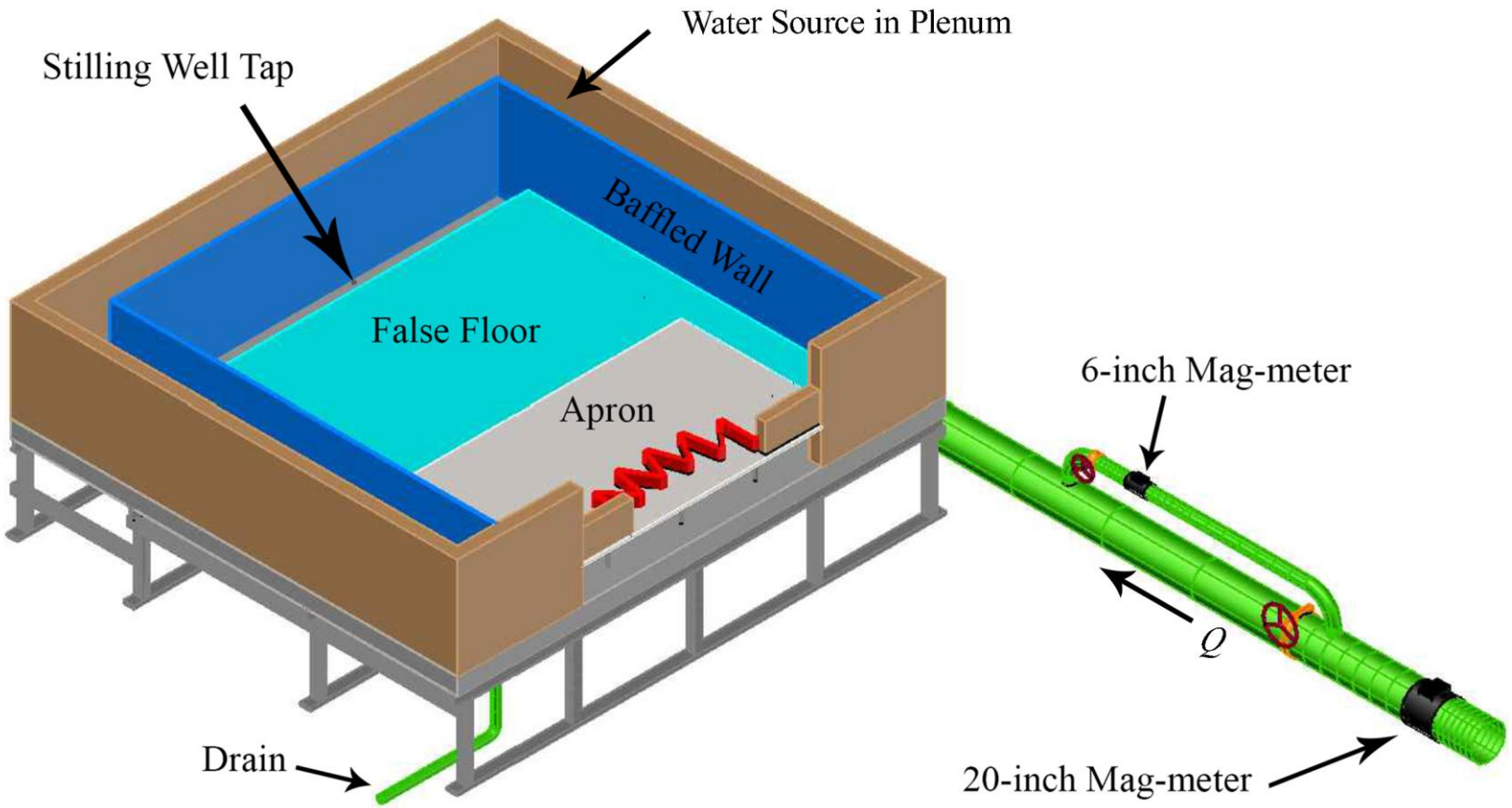

Fig. A2. Headbox 3D schematic.

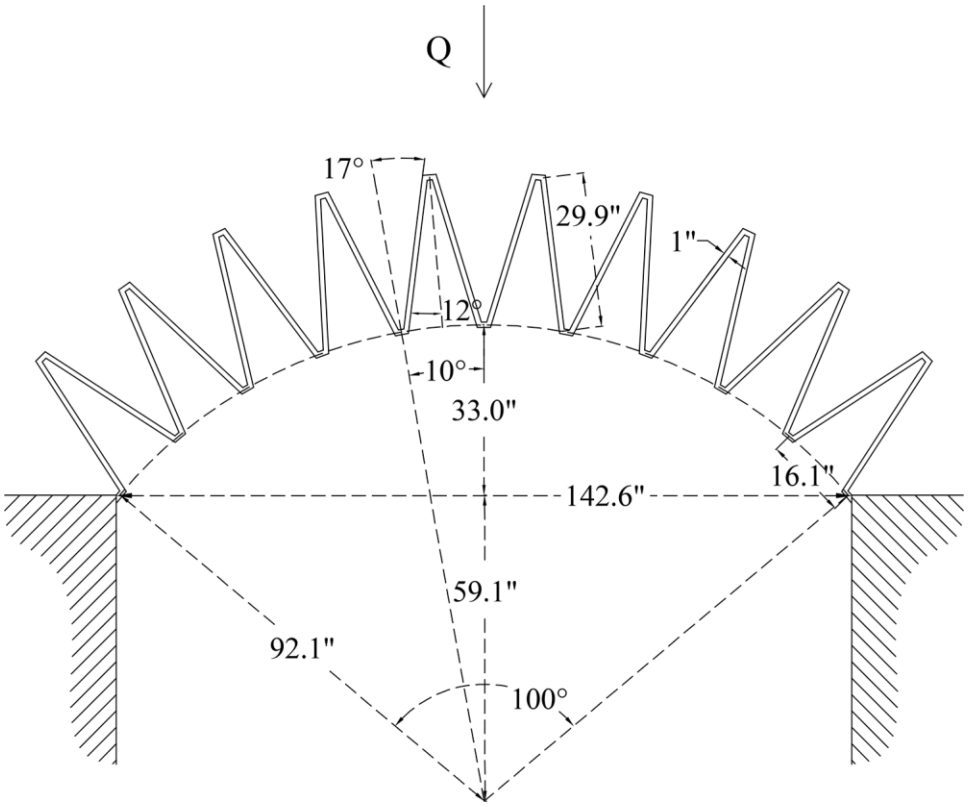

Fig. A3. 10-cycle, α = 12°, θ = 10°, schematic.

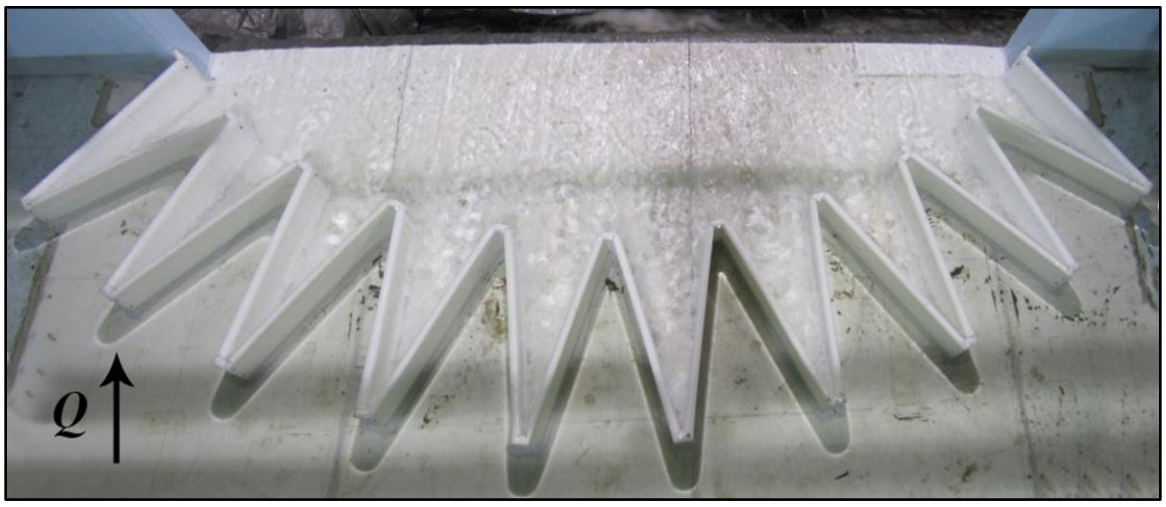

Fig. A4. 10-cycle, α = 12°, θ = 10°, photograph.

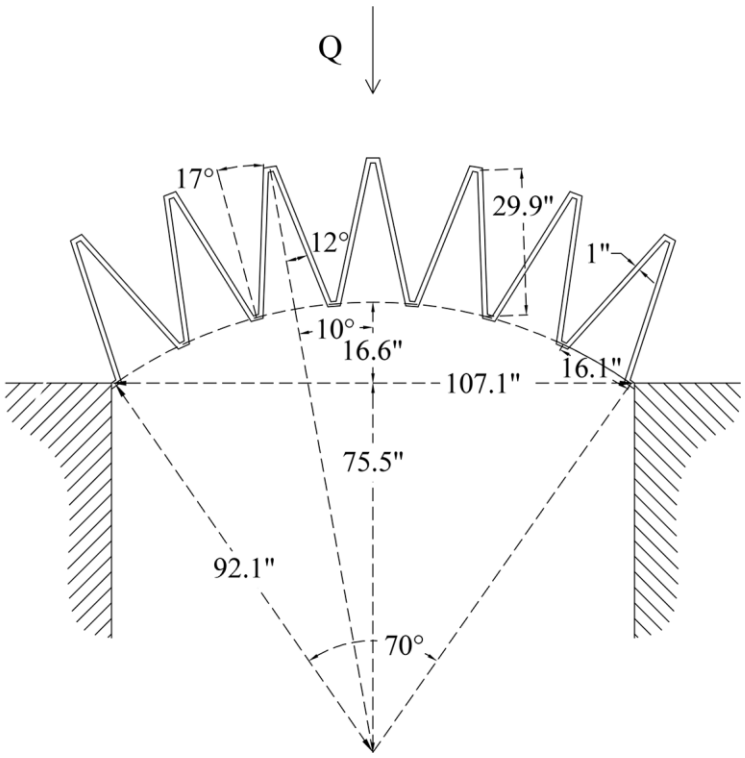

Fig. A5. 7-cycle, α = 12°, θ = 10°, schematic.

Fig. A6. 7-cycle, α = 12°, θ = 10°, photograph.

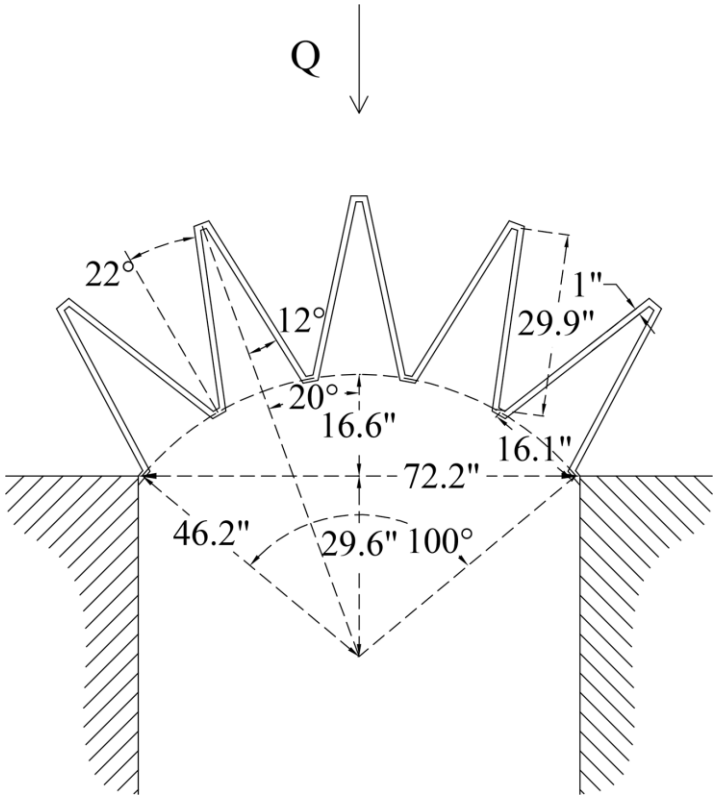

Fig. A7. 5-cycle, α = 12°, θ = 20°, schematic.

Fig. A8. 5-cycle, α = 12°, θ = 20°, photograph.

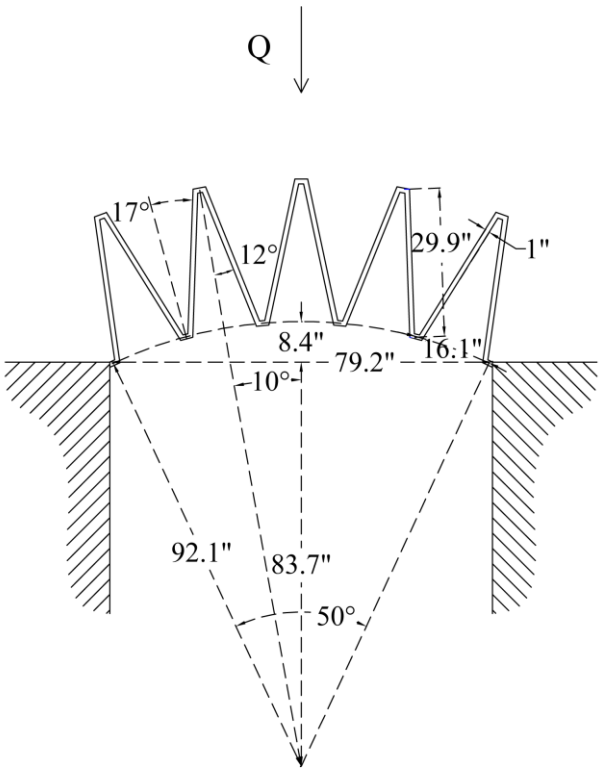

Fig. A9. 5-cycle, α = 12°, θ = 10°, schematic.

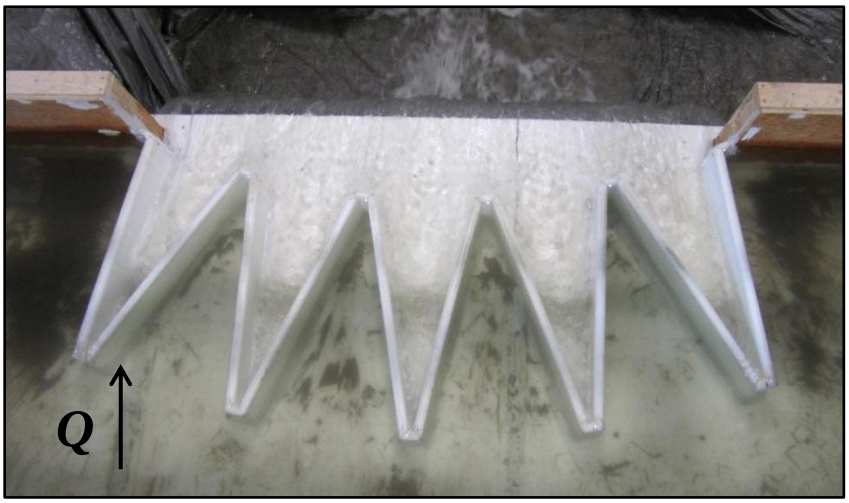

Fig. A10. 5-cycle, α = 12°, θ = 10°, photograph.

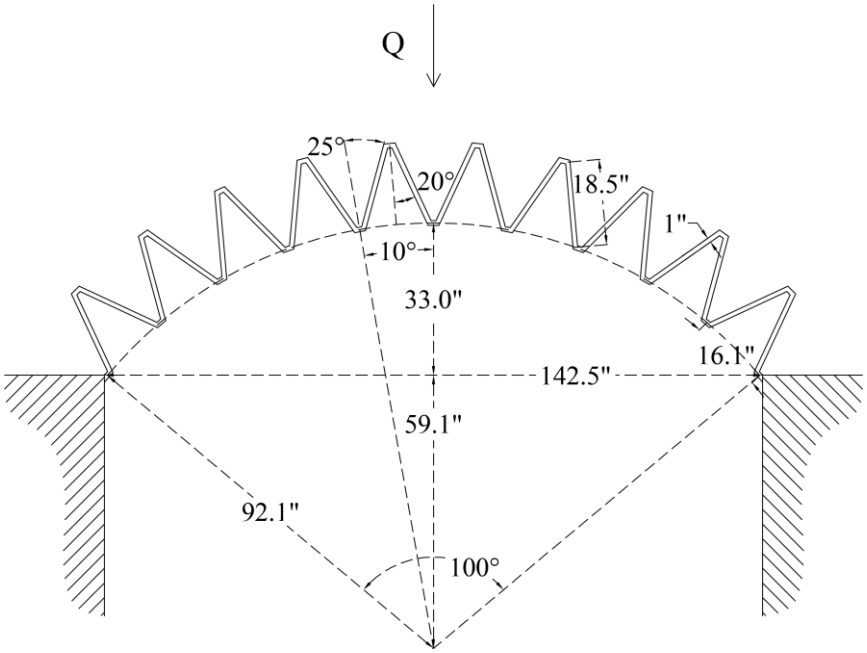

Fig. A11. 10-cycle, α = 20°, θ = 10°, schematic.

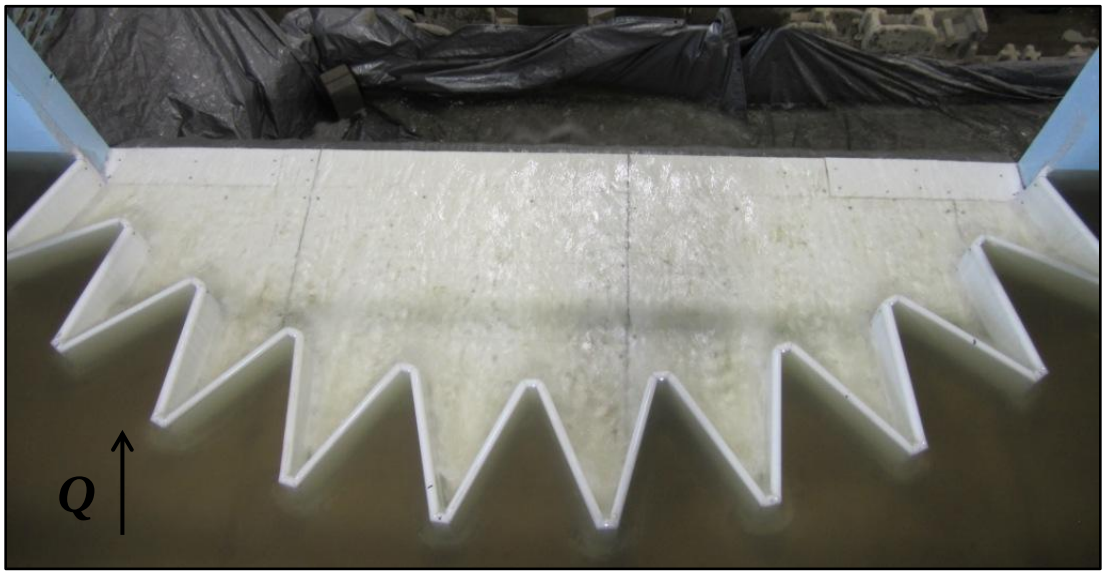

Fig. A12. 10-cycle, α = 20°, θ = 10°, photograph.

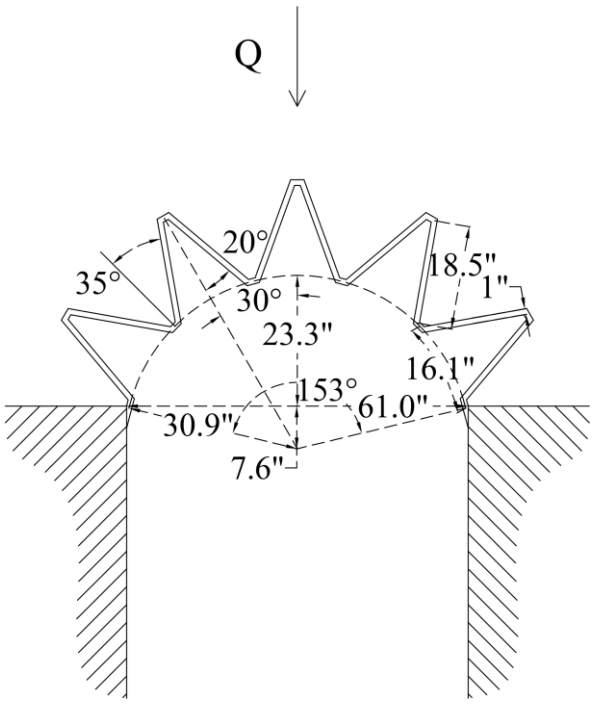

Fig. A13. 5-cycle, α = 20°, θ = 30°, schematic.

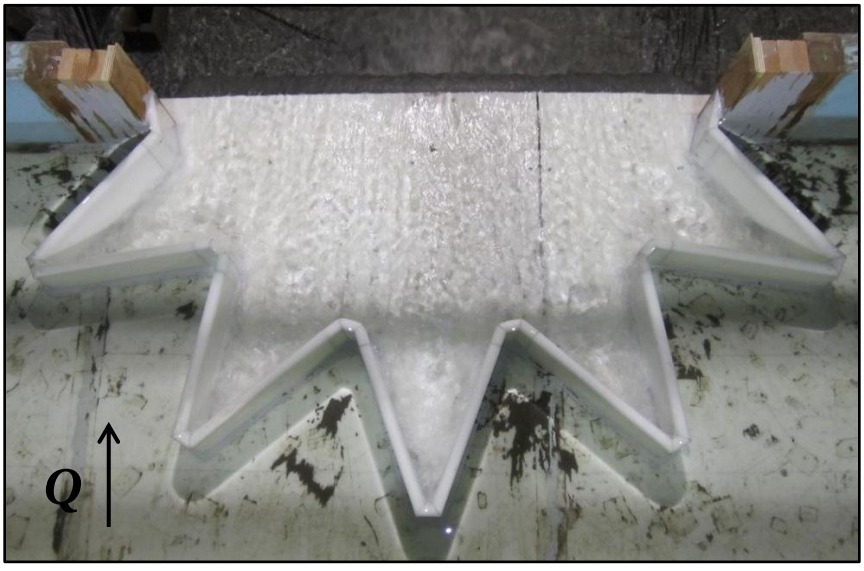

Fig. A14. 5-cycle, α = 20°, θ = 30°, photograph.

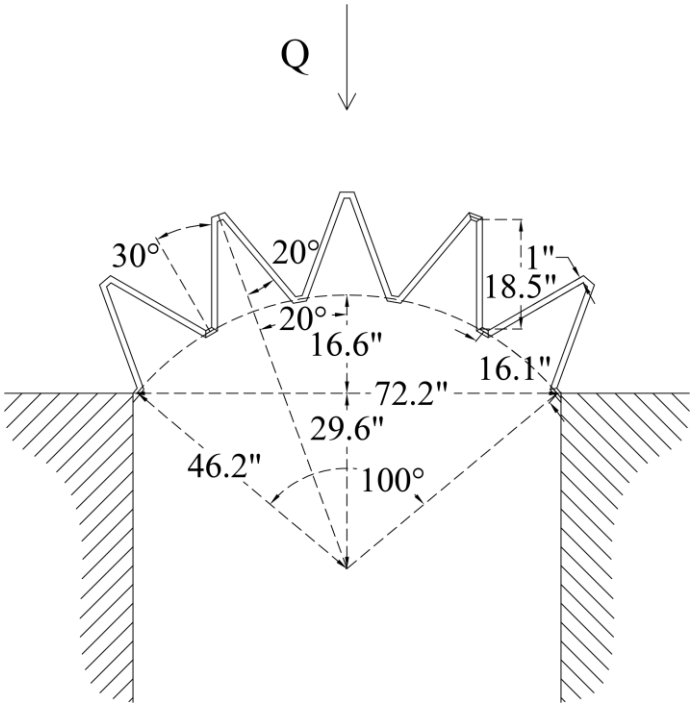

Fig. A15. 5-cycle, α = 20°, θ = 20°, schematic.

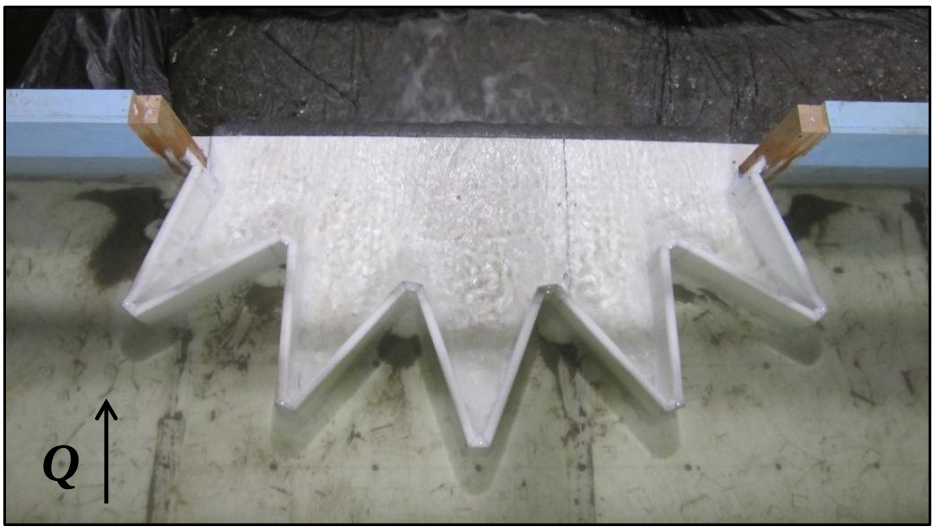

Fig. A16. 5-cycle, α = 20°, θ = 20°, photograph.

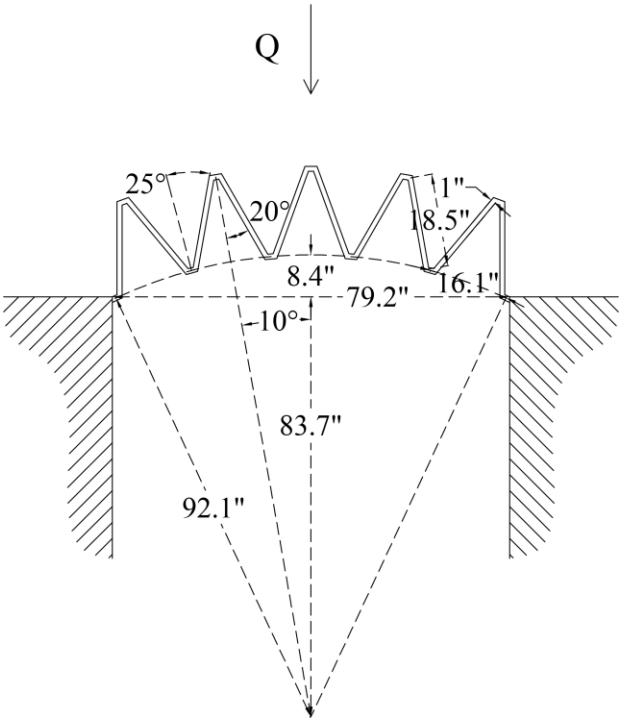

Fig. A17. 5-cycle, α = 20°, θ = 10°, schematic.

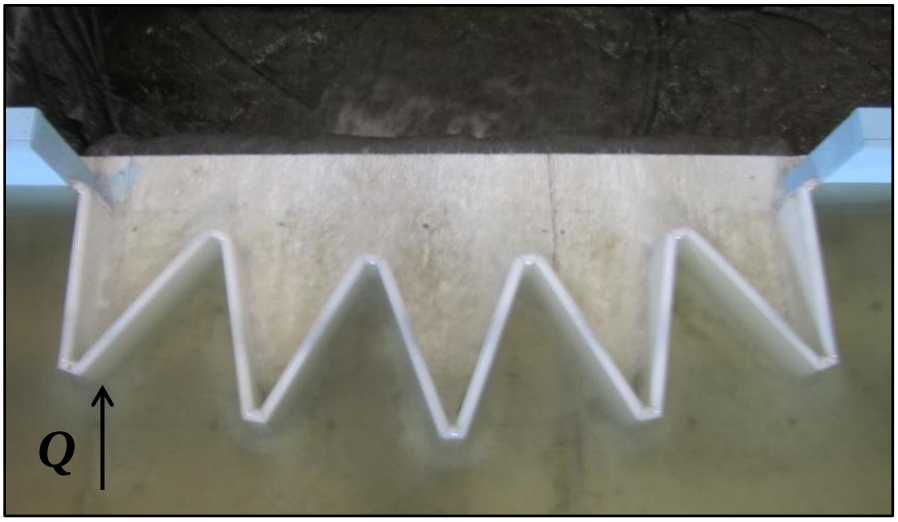

Fig. A18. 5-cycle, α = 20°, θ = 10°, photograph.

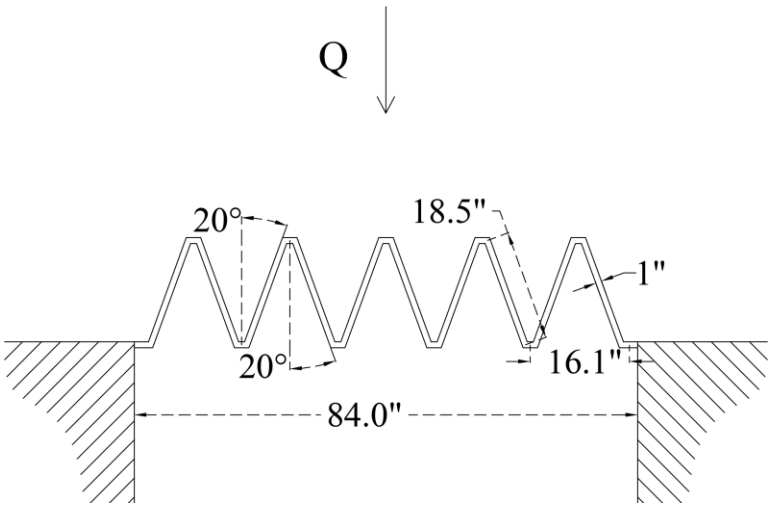

Fig. A19. 5-cycle, α = 20°, θ = 0° projecting, schematic.

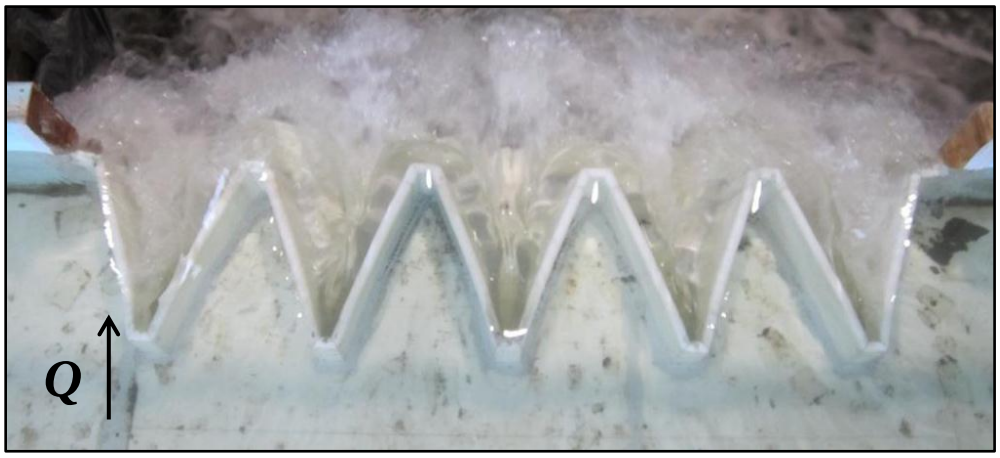

Fig. A20. 5-cycle, α = 20°, θ = 0° projecting, photograph.

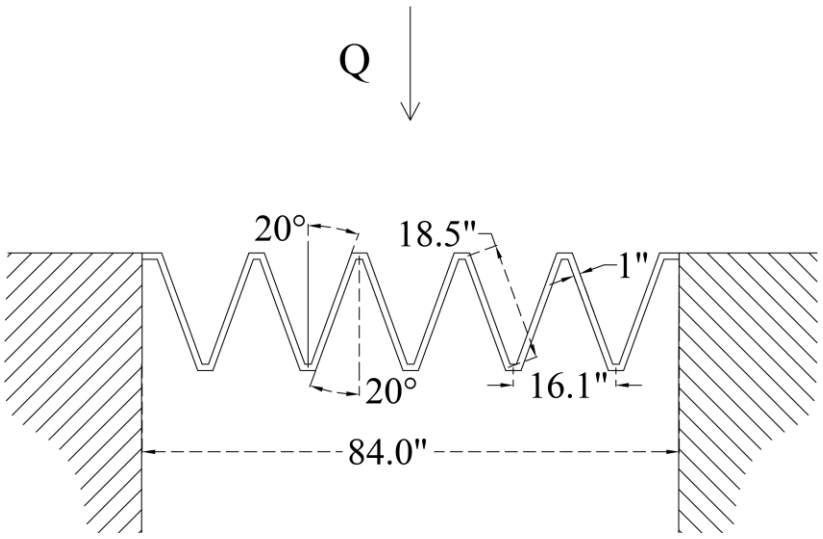

Fig. A21. 5-cycle, α = 20°, θ = 0° flush, schematic.

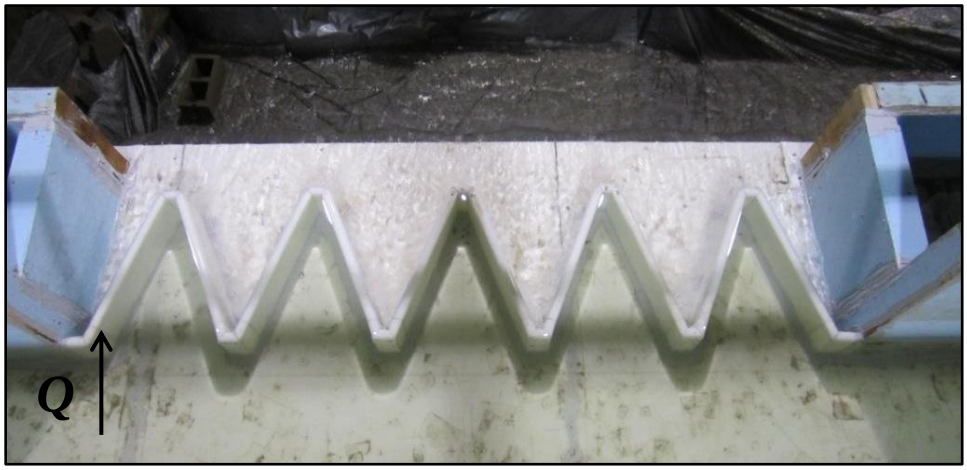

Fig. A22. 5-cycle, α = 20°, θ = 0° flush, photograph.

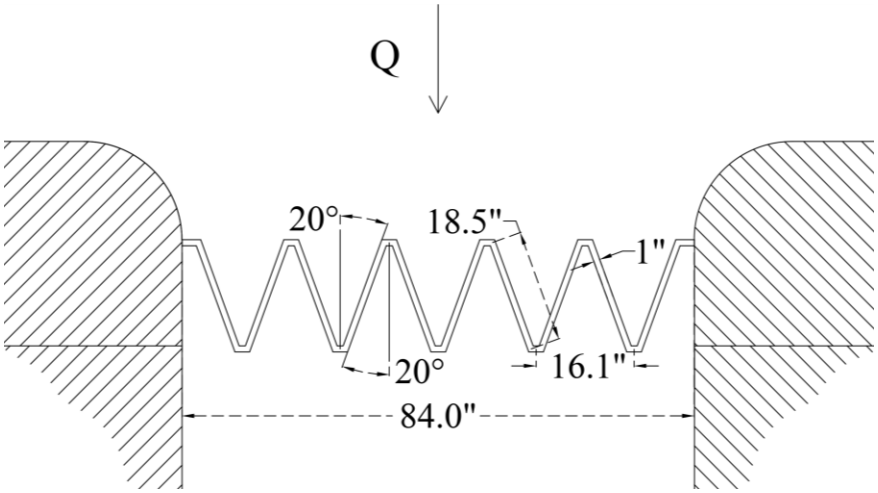

Fig. A23. 5-cycle, α = 20°, θ = 0° rounded inlet, schematic.

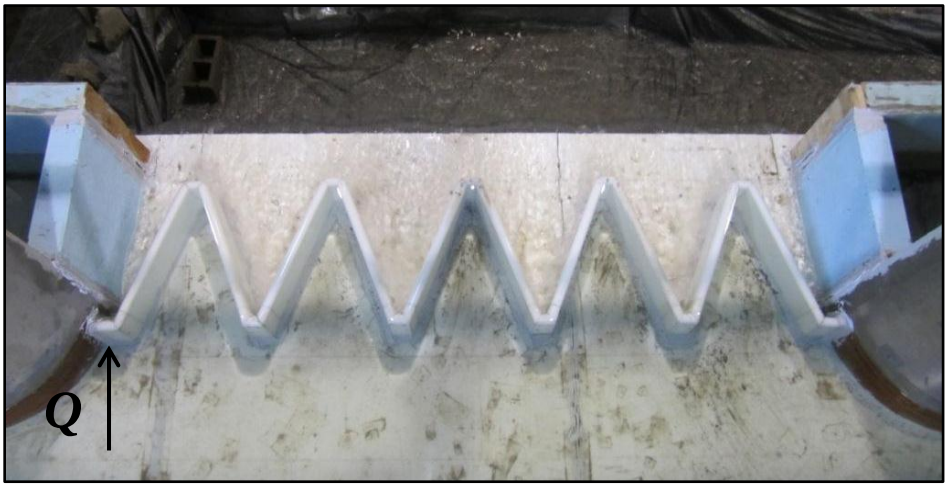

Fig. A24. 5-cycle, α = 20°, θ = 0° rounded inlet, photograph.

APPENDIX B

Data

Table B1. 10-cycle, α = 12°, θ = 10° data.

P (in) =	7.969	t_w (in) =	0.984	N =	10
L_c (in) =	634	W (in) =	142.551	R (in) =	92.094
Q (cfs)	H_T (ft)	H_T/P	C_d	Measurement Uncertainty (%)	± Error Bars
		Without	Breakers		
2.987	0.063	0.095	0.672	2.855%	0.019
3.636	0.071	0.107	0.684	2.497%	0.017
4.048	0.076	0.114	0.687	2.325%	0.016
4.152	0.077	0.116	0.691	2.283%	0.016
4.494	0.082	0.123	0.680	2.181%	0.015
5.509	0.093	0.140	0.685	1.909%	0.013
6.330	0.103	0.155	0.675	1.757%	0.012
7.118	0.112	0.169	0.670	1.636%	0.011
8.764	0.129	0.195	0.667	1.440%	0.009
9.915	0.142	0.213	0.657	1.343%	0.009
11.151	0.155	0.233	0.648	1.259%	0.008
11.950	0.164	0.247	0.635	1.218%	0.008
13.970	0.187	0.281	0.613	1.131%	0.007
15.560	0.205	0.309	0.592	1.081%	0.006
16.969	0.222	0.335	0.573	1.047%	0.006
17.817	0.233	0.351	0.562	1.030%	0.006
		With	Breakers		
2.941	0.062	0.094	0.670	2.888%	0.019
4.072	0.077	0.116	0.678	2.328%	0.016
5.501	0.093	0.140	0.684	1.912%	0.013
7.395	0.114	0.172	0.678	1.591%	0.011
8.028	0.123	0.185	0.661	1.526%	0.010
8.615	0.131	0.197	0.645	1.474%	0.009
9.793	0.144	0.217	0.633	1.374%	0.009
10.730	0.156	0.235	0.618	1.313%	0.008
13.692	0.188	0.283	0.593	1.159%	0.007
15.265	0.206	0.310	0.579	1.103%	0.006
16.585	0.220	0.332	0.568	1.064%	0.006
18.042	0.239	0.360	0.546	1.037%	0.005

Table B2. 7-cycle, α = 12°, θ = 10° data.

P (in) =	8.063	t_w (in) =	0.991	N =	7
L_c (in) =	447	W (in) =	107.096	R (in) =	92.094
Q (cfs)	H_T (ft)	H_T/P	C_d	Measurement Uncertainty (%)	± Error Bars
Without Breakers					
2.467	0.070	0.104	0.675	2.572%	0.017
2.946	0.078	0.116	0.678	2.288%	0.015
3.348	0.085	0.127	0.677	2.108%	0.014
4.096	0.098	0.145	0.674	1.855%	0.012
4.513	0.104	0.155	0.675	1.744%	0.012
5.394	0.118	0.176	0.667	1.565%	0.010
6.122	0.129	0.192	0.663	1.451%	0.009
6.947	0.141	0.210	0.658	1.347%	0.009
7.815	0.155	0.230	0.645	1.265%	0.008
8.653	0.168	0.249	0.633	1.200%	0.007
9.148	0.175	0.261	0.627	1.167%	0.007
9.836	0.186	0.277	0.615	1.128%	0.007
10.733	0.200	0.297	0.604	1.083%	0.006
12.305	0.227	0.337	0.573	1.030%	0.006
12.971	0.238	0.354	0.560	1.012%	0.006
14.088	0.260	0.386	0.535	0.993%	0.005
15.497	0.288	0.428	0.504	0.976%	0.005
16.131	0.299	0.445	0.495	0.968%	0.005
With Breakers					
2.931	0.078	0.116	0.674	2.300%	0.015
4.658	0.107	0.159	0.672	1.712%	0.011
5.593	0.124	0.184	0.646	1.549%	0.010
6.358	0.137	0.203	0.632	1.443%	0.009
7.374	0.154	0.229	0.615	1.334%	0.008
8.608	0.173	0.258	0.600	1.230%	0.007
9.991	0.194	0.289	0.587	1.141%	0.007
10.963	0.209	0.311	0.576	1.093%	0.006
12.325	0.230	0.342	0.561	1.039%	0.006
13.761	0.255	0.379	0.538	1.001%	0.005

Table B3. 5-cycle, α = 12°, θ = 20° data.

P (in) =	8.000	t_w (in) =	0.983	N =	5
L_c (in) =	318	W (in) =	72	R (in)=	46.169
Q (cfs)	H_T (ft)	H_T/P	C_d	Measurement Uncertainty (%)	± Error Bars
Without Breakers					
1.529	0.062	0.094	0.692	2.250%	0.016
1.683	0.067	0.100	0.686	2.093%	0.014
2.015	0.074	0.111	0.707	1.794%	0.013
2.358	0.081	0.122	0.716	1.608%	0.011
2.846	0.092	0.138	0.721	1.469%	0.010
2.952	0.094	0.141	0.724	1.794%	0.013
3.888	0.112	0.168	0.733	1.501%	0.011
4.535	0.125	0.187	0.725	1.370%	0.010
5.328	0.140	0.210	0.718	1.246%	0.009
6.022	0.152	0.228	0.718	1.158%	0.008
6.941	0.171	0.257	0.690	1.082%	0.007
8.203	0.199	0.298	0.652	1.009%	0.006
9.654	0.218	0.327	0.626	0.955%	0.006
10.504	0.232	0.349	0.608	0.935%	0.005
11.175	0.253	0.380	0.581	0.922%	0.005
12.450	0.270	0.405	0.562	0.910%	0.005
13.880	0.304	0.456	0.524	0.910%	0.004
14.933	0.345	0.518	0.482	0.919%	0.004
19.608	0.378	0.568	0.453	0.987%	0.003
With Breakers					
1.537	0.062	0.094	0.695	2.237%	0.015
2.023	0.074	0.112	0.703	1.796%	0.013
2.674	0.088	0.132	0.724	1.500%	0.011
3.278	0.100	0.151	0.727	1.676%	0.012
4.044	0.116	0.174	0.723	1.472%	0.010
4.406	0.125	0.188	0.700	1.413%	0.010
4.957	0.137	0.206	0.687	1.324%	0.009
6.003	0.159	0.238	0.669	1.193%	0.008
7.597	0.189	0.283	0.653	1.052%	0.007
9.065	0.219	0.328	0.624	0.974%	0.006

Table B4. 5-cycle, α = 12°, θ = 10° data.

P (in) =	8.031	t_w (in) =	0.997	N =	5
L_c (in) =	317.35	W (in) =	79	R (in)=	92.094
Q (cfs)	H_T (ft)	H_T/P	C_d	Measurement Uncertainty (%)	± Error Bars
Without Breakers					
1.584	0.065	0.097	0.682	2.26%	0.015
1.912	0.073	0.109	0.691	1.94%	0.013
2.356	0.082	0.123	0.708	1.65%	0.012
2.882	0.094	0.141	0.706	1.48%	0.010
3.704	0.112	0.167	0.702	1.57%	0.011
4.806	0.136	0.203	0.680	1.35%	0.009
4.106	0.120	0.179	0.702	1.47%	0.010
5.960	0.160	0.239	0.661	1.20%	0.008
7.095	0.183	0.273	0.643	1.10%	0.007
8.280	0.207	0.309	0.621	1.02%	0.006
9.446	0.237	0.354	0.580	0.98%	0.006
10.592	0.268	0.400	0.541	0.96%	0.005
11.789	0.300	0.448	0.508	0.94%	0.005
14.305	0.370	0.552	0.450	0.93%	0.004
16.526	0.434	0.648	0.409	0.94%	0.004
With Breakers					
1.693	0.067	0.100	0.686	2.616%	0.018
2.362	0.083	0.124	0.701	2.092%	0.015
2.977	0.096	0.144	0.704	1.801%	0.013
3.455	0.106	0.158	0.710	1.634%	0.011
4.020	0.119	0.178	0.690	1.501%	0.010
4.733	0.137	0.204	0.661	1.379%	0.009
5.398	0.152	0.227	0.645	1.286%	0.008
6.277	0.170	0.254	0.634	1.185%	0.007
6.955	0.183	0.273	0.629	1.121%	0.007
7.735	0.198	0.296	0.619	1.063%	0.006
8.855	0.224	0.334	0.591	1.008%	0.006
10.124	0.254	0.380	0.558	0.967%	0.005

Table B5. 10-cycle, α = 20°, θ = 10° data.

P (in) =	8.016	t_w (in) =	0.988	N =	10
L_c (in) =	405.6875	W (in) =	142.375	R (in)=	92.097
Q (cfs)	H_T (ft)	H_T/P	C_d	Measurement Uncertainty (%)	± Error Bars
		Without	Breakers		
1.940	0.065	0.097	0.654	2.852%	0.019
2.135	0.069	0.103	0.658	2.675%	0.018
2.327	0.072	0.108	0.665	2.519%	0.017
2.758	0.080	0.119	0.679	2.239%	0.015
2.996	0.084	0.125	0.686	2.116%	0.014
3.686	0.096	0.143	0.690	1.847%	0.013
4.002	0.101	0.151	0.689	1.754%	0.012
5.296	0.121	0.181	0.695	1.465%	0.010
6.891	0.145	0.216	0.693	1.247%	0.009
7.906	0.159	0.238	0.689	1.151%	0.008
8.313	0.165	0.246	0.689	1.118%	0.008
9.442	0.182	0.273	0.672	1.048%	0.007
10.919	0.205	0.307	0.650	0.979%	0.006
11.968	0.221	0.331	0.637	0.940%	0.006
12.594	0.231	0.345	0.629	0.919%	0.006
14.088	0.253	0.379	0.612	0.879%	0.005
		With	Breakers		
2.142	0.069	0.103	0.660	2.667%	0.018
2.672	0.078	0.117	0.677	2.288%	0.015
3.619	0.094	0.141	0.694	1.866%	0.013
4.502	0.111	0.166	0.677	1.638%	0.011
5.525	0.129	0.192	0.663	1.453%	0.010
6.425	0.145	0.216	0.646	1.337%	0.009
7.354	0.160	0.240	0.635	1.241%	0.008
8.647	0.181	0.270	0.623	1.138%	0.007
10.984	0.217	0.324	0.603	1.009%	0.006
13.190	0.249	0.372	0.589	0.926%	0.005
14.994	0.276	0.413	0.572	0.881%	0.005
18.079	0.323	0.483	0.546	0.827%	0.004
22.059	0.379	0.568	0.523	0.781%	0.004

Table B6. 5-cycle, α = 20°, θ = 30° data.

P (in) =	8	t_w (in) =	1	N =	5
L_c (in) =	206.928	W (in) =	60.931	R (in)=	30.910
Q (cfs)	H_T (ft)	H_T/P	C_d	Measurement Uncertainty (%)	± Error Bars
Without Breakers					
1.084	0.068	0.102	0.660	2.306%	0.015
1.331	0.077	0.115	0.679	1.939%	0.013
1.558	0.084	0.126	0.698	1.701%	0.012
1.870	0.094	0.141	0.707	1.497%	0.011
2.183	0.103	0.154	0.719	1.369%	0.010
2.350	0.108	0.162	0.721	1.329%	0.010
2.663	0.117	0.176	0.720	1.291%	0.009
3.110	0.130	0.195	0.718	1.328%	0.009
3.850	0.149	0.223	0.728	1.160%	0.008
4.508	0.167	0.250	0.718	1.062%	0.008
5.085	0.181	0.271	0.718	0.990%	0.007
5.677	0.198	0.297	0.698	0.942%	0.006
6.472	0.221	0.331	0.677	0.889%	0.006
7.230	0.242	0.363	0.658	0.850%	0.005
7.968	0.264	0.396	0.638	0.822%	0.005
8.648	0.284	0.426	0.619	0.802%	0.005
9.485	0.311	0.466	0.594	0.786%	0.005
10.316	0.338	0.507	0.570	0.776%	0.004
11.631	0.383	0.575	0.532	0.771%	0.004
13.114	0.442	0.663	0.484	0.785%	0.004
15.337	0.547	0.820	0.411	0.838%	0.003
With Breakers					
1.893	0.096	0.144	0.693	1.501%	0.010
2.245	0.106	0.159	0.708	1.365%	0.010
2.863	0.114	0.171	0.699	1.426%	0.010
3.854	0.128	0.192	0.681	1.206%	0.008
5.102	0.159	0.239	0.658	1.028%	0.007
6.335	0.193	0.289	0.654	0.916%	0.006
7.230	0.224	0.336	0.649	0.859%	0.005

Table B7. 5-cycle, α = 20°, θ = 20° data.

P (in) =	8	t_w (in) =	0.988	N =	5
L_c (in) =	203.950	W (in) =	72	R (in)=	46.169
Q (cfs)	H_T (ft)	H_T/P	C_d	Measurement Uncertainty (%)	± Error Bars
Without Breakers					
0.974	0.065	0.096	0.653	2.858%	0.019
1.423	0.081	0.120	0.685	2.195%	0.015
1.913	0.096	0.143	0.707	1.795%	0.013
2.292	0.108	0.160	0.715	1.594%	0.011
2.907	0.126	0.186	0.719	1.370%	0.010
3.126	0.132	0.196	0.717	1.311%	0.009
3.790	0.149	0.221	0.725	1.161%	0.008
4.059	0.157	0.233	0.721	1.117%	0.008
4.270	0.165	0.244	0.704	1.094%	0.008
5.691	0.204	0.302	0.682	0.940%	0.006
6.383	0.222	0.329	0.673	0.888%	0.006
7.055	0.241	0.358	0.656	0.852%	0.005
8.303	0.278	0.412	0.625	0.804%	0.005
9.414	0.311	0.461	0.598	0.776%	0.005
10.900	0.357	0.530	0.563	0.754%	0.004
12.528	0.406	0.603	0.533	0.739%	0.004
13.802	0.447	0.663	0.509	0.736%	0.004
15.515	0.507	0.752	0.473	0.746%	0.003
16.727	0.547	0.812	0.455	0.753%	0.003
18.143	0.581	0.863	0.451	0.744%	0.003
With Breakers					
1.308	0.077	0.114	0.679	2.326%	0.016
1.723	0.091	0.134	0.695	1.931%	0.013
2.227	0.108	0.160	0.694	1.640%	0.011
2.877	0.129	0.192	0.683	1.406%	0.010
3.366	0.145	0.215	0.670	1.286%	0.009
4.082	0.167	0.247	0.661	1.152%	0.008
5.395	0.208	0.308	0.628	1.004%	0.006
8.050	0.282	0.418	0.593	0.838%	0.005
9.382	0.318	0.472	0.577	0.792%	0.004

Table B8. 5-cycle, α = 20°, θ = 10° data.

P (in) =	8.100	t_w (in) =	0.988	N =	5
L_c (in) =	206.240	W (in) =	79	R (in)=	92.097
Q (cfs)	H_T (ft)	H_T/P	C_d	Measurement Uncertainty (%)	± Error Bars
Without Breakers					
0.975	0.064	0.095	0.658	2.866%	0.019
1.132	0.070	0.104	0.661	2.597%	0.017
2.086	0.102	0.151	0.699	1.717%	0.012
2.642	0.119	0.176	0.702	1.477%	0.010
3.058	0.132	0.195	0.695	1.353%	0.009
3.498	0.145	0.215	0.687	1.252%	0.009
3.772	0.154	0.228	0.680	1.201%	0.008
4.044	0.161	0.238	0.682	1.151%	0.008
4.415	0.175	0.260	0.654	1.111%	0.007
5.358	0.202	0.300	0.641	1.004%	0.006
6.003	0.220	0.326	0.632	0.949%	0.006
6.602	0.237	0.351	0.623	0.908%	0.006
7.902	0.273	0.405	0.602	0.842%	0.005
8.852	0.302	0.447	0.581	0.813%	0.005
9.921	0.336	0.498	0.553	0.793%	0.004
11.123	0.369	0.547	0.539	0.768%	0.004
12.254	0.406	0.601	0.516	0.760%	0.004
13.768	0.455	0.675	0.488	0.757%	0.004
16.272	0.541	0.801	0.445	0.767%	0.003
18.205	0.589	0.873	0.438	0.756%	0.003
With Breakers					
1.730	0.091	0.135	0.688	1.946%	0.013
2.623	0.120	0.177	0.688	1.495%	0.010
3.213	0.141	0.209	0.662	1.338%	0.009
3.746	0.158	0.234	0.650	1.228%	0.008
4.101	0.169	0.250	0.643	1.169%	0.007
4.393	0.180	0.266	0.627	1.135%	0.007
5.393	0.209	0.310	0.613	1.020%	0.006
6.857	0.251	0.372	0.594	0.910%	0.005
8.304	0.291	0.432	0.575	0.842%	0.005

Table B9. 5-cycle, α = 20°, θ = 0°, projecting data.

P (in) =	7.938	t_w (in) =	0.997	N =	5
L_c (in) =	203.500	W (in) =	85	R (in)=	0
Q (cfs)	H_T (ft)	H_T/P	C_d	Measurement Uncertainty (%)	± Error Bars
		Without	Breakers		
0.955	0.065	0.098	0.638	2.714%	0.017
1.055	0.068	0.103	0.651	2.502%	0.016
1.217	0.075	0.113	0.656	2.243%	0.015
1.372	0.080	0.121	0.664	2.039%	0.014
1.518	0.085	0.129	0.671	1.882%	0.013
1.775	0.094	0.142	0.681	1.666%	0.011
1.924	0.099	0.149	0.683	1.570%	0.011
2.121	0.105	0.158	0.689	1.460%	0.010
2.646	0.121	0.183	0.690	1.275%	0.009
3.143	0.139	0.210	0.670	1.338%	0.009
3.744	0.158	0.239	0.658	1.212%	0.008
4.374	0.177	0.267	0.649	1.112%	0.007
5.123	0.200	0.303	0.630	1.029%	0.006
6.361	0.237	0.359	0.607	0.930%	0.006
7.587	0.275	0.415	0.581	0.868%	0.005
8.703	0.310	0.468	0.556	0.831%	0.005
9.826	0.345	0.521	0.535	0.805%	0.004
11.029	0.385	0.582	0.509	0.790%	0.004
12.200	0.425	0.643	0.485	0.785%	0.004
13.866	0.479	0.725	0.461	0.778%	0.004
16.003	0.547	0.827	0.436	0.776%	0.003

Table B10. 5-cycle, α = 20°, θ = 0°, flush data.

P (in) =	7.938	t_w (in) =	0.997	N =	5
L_c (in) =	203.500	W (in) =	85	R (in)=	0
Q (cfs)	H_T (ft)	H_T/P	C_d	Measurement Uncertainty (%)	± Error Bars
Without Breakers					
0.991	0.066	0.099	0.649	2.622%	0.017
1.135	0.071	0.108	0.659	2.357%	0.016
1.370	0.080	0.120	0.671	2.032%	0.014
1.592	0.087	0.132	0.682	1.804%	0.012
1.788	0.095	0.143	0.677	1.662%	0.011
1.979	0.101	0.152	0.683	1.538%	0.010
2.211	0.108	0.164	0.685	1.425%	0.010
2.457	0.117	0.176	0.679	1.340%	0.009
2.696	0.124	0.187	0.683	1.270%	0.009
2.888	0.130	0.197	0.678	1.235%	0.008
3.713	0.157	0.238	0.657	1.219%	0.008
4.778	0.190	0.288	0.635	1.066%	0.007
6.031	0.230	0.347	0.604	0.958%	0.006
7.204	0.269	0.407	0.569	0.900%	0.005
8.362	0.308	0.466	0.539	0.861%	0.005
9.535	0.347	0.525	0.514	0.834%	0.004
10.818	0.390	0.589	0.490	0.814%	0.004
11.996	0.430	0.650	0.469	0.806%	0.004
14.377	0.509	0.770	0.436	0.798%	0.003
16.692	0.585	0.885	0.411	0.800%	0.003

Table B11. 5-cycle, α = 20°, θ = 0°, rounded inlet data.

P (in) =	7.938	t_w (in) =	0.997	N =	5
L_c (in) =	203.500	W (in) =	85	R (in)=	0
Q (cfs)	H_T (ft)	H_T/P	C_d	Measurement Uncertainty (%)	± Error Bars
Without Breakers					
0.898	0.062	0.094	0.637	2.840%	0.018
1.059	0.069	0.104	0.647	2.501%	0.016
1.336	0.079	0.119	0.666	2.078%	0.014
1.553	0.086	0.130	0.675	1.845%	0.012
1.776	0.094	0.142	0.682	1.664%	0.011
2.031	0.102	0.155	0.684	1.510%	0.010
2.233	0.108	0.164	0.691	1.410%	0.010
2.442	0.115	0.174	0.688	1.337%	0.009
2.684	0.123	0.185	0.689	1.267%	0.009
2.888	0.129	0.195	0.689	1.224%	0.008
3.004	0.133	0.201	0.684	1.365%	0.009
3.756	0.154	0.233	0.687	1.190%	0.008
4.848	0.187	0.282	0.662	1.039%	0.007
5.106	0.195	0.295	0.652	1.015%	0.007
5.214	0.199	0.301	0.649	1.006%	0.006
6.095	0.225	0.341	0.628	0.936%	0.006
7.019	0.253	0.382	0.609	0.882%	0.005
7.457	0.267	0.404	0.595	0.865%	0.005
8.589	0.301	0.456	0.573	0.824%	0.005
9.451	0.326	0.493	0.559	0.799%	0.004
11.244	0.381	0.576	0.528	0.768%	0.004
11.811	0.398	0.602	0.518	0.762%	0.004
13.719	0.462	0.698	0.482	0.757%	0.004
15.159	0.509	0.770	0.460	0.758%	0.003
17.045	0.568	0.859	0.439	0.760%	0.003

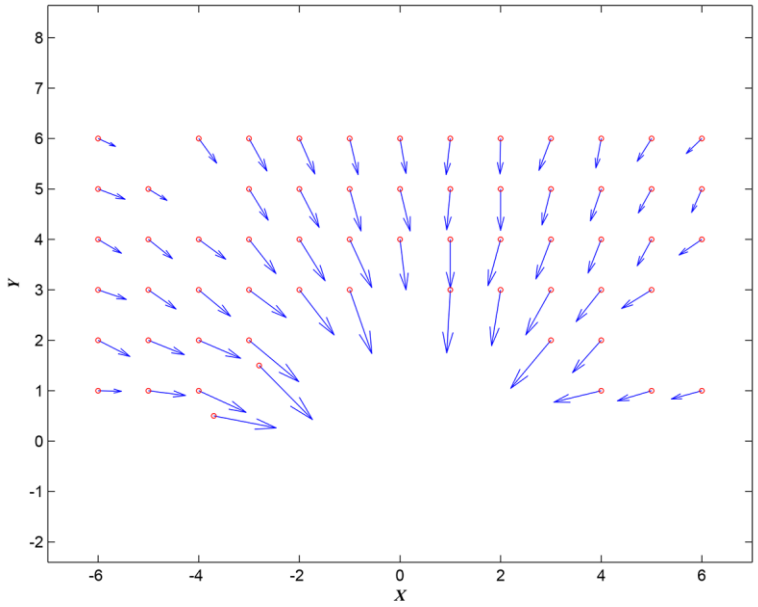

Fig B1. 10-cycle, α = 12º, θ = 10º velocity grid at H_T/P = 0.3.

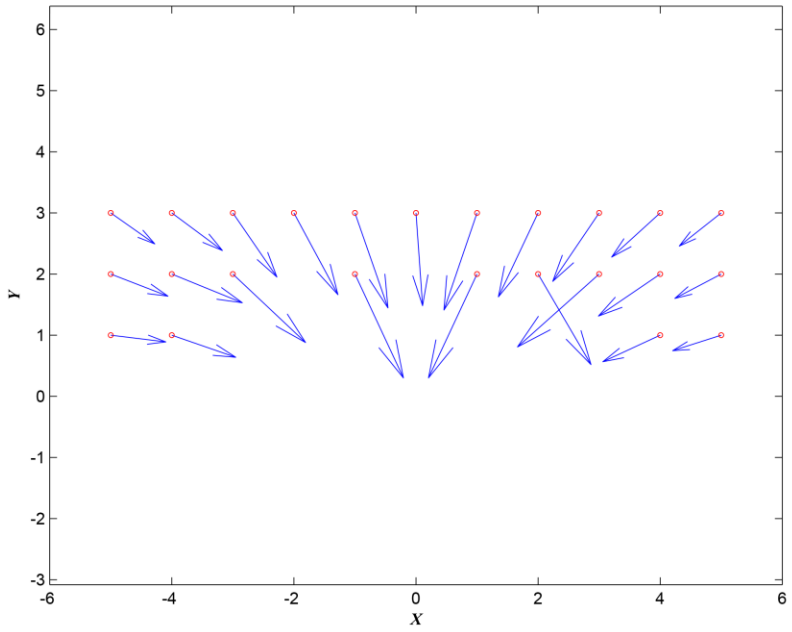

Fig B2. 5-cycle, α = 12º, θ = 10º velocity grid at H_T/P = 0.3.

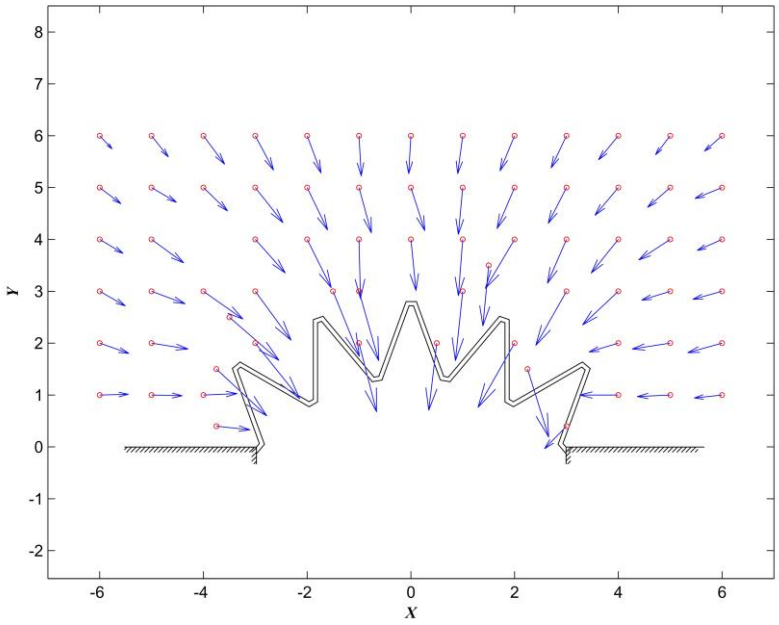

Fig B3. 5-cycle, α = 20º, θ = 20º velocity grid at H_T/P = 0.3.

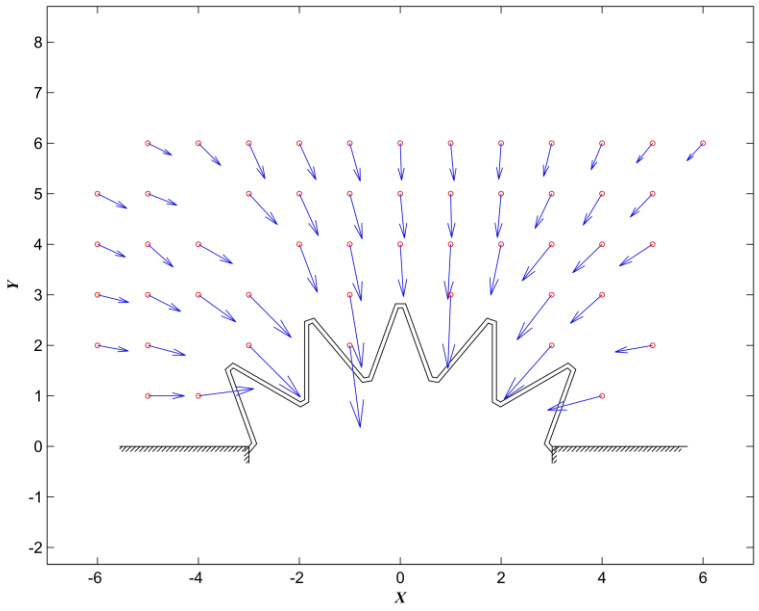

Fig B4. 5-cycle, α = 20º, θ = 20º velocity grid at H_T/P = 0.6.

APPENDIX C

Microsoft Excel VBA Code

Specific to UWRL Headbox Facility

```
‘Headbox Flow Function (with orifice plates)
'For use with reservoir/headbox on lower floor level (UWRL) with orifice plates
    Public Function flowtRes(Size, dH, g, leak)
    Dim beta, a, Dorifice, Dpipe, pi, C, Calib As Double
    pi = 3.14159265359
'Calculate Q in Headbox (with orifice plates)
    If (Size = 4) Then
        C = 0.6197
        a = 1.5 ^ 2 * 3.14159 * 0.25 / 144
        beta = 1.5 / 4.026
        flowtRes = (C * a * (2 * g * dH) ^ 0.5 / (1 - beta ^ 4) ^ 0.5) - leak
    ElseIf (Size = 8) Then
        C = 0.6106
        a = 5 ^ 2 * 3.14159 * 0.25 / 144
        beta = 5 / 7.981
        Calib = 1
        flowtRes = (C * a * (2 * g * dH) ^ 0.5 / (1 - beta ^ 4) ^ 0.5) * Calib - leak
    ElseIf (Size = 20) Then
        C = 0.6029
        a = 14.016 ^ 2 * 3.14159 * 0.25 / 144
        beta = 14.016 / 19.25
        flowtRes = (C * a * (2 * g * dH) ^ 0.5 / (1 - beta ^ 4) ^ 0.5)
```

```
        Calib = 1 - (0.000071079566 * flowtRes ^ 2 - 0.002182705515 * flowtRes +
            0.024449497333)

        flowtRes = flowtRes * Calib - leak
    Else: flowtRes = "Check Meter!"
    End If
    End Function


'Headbox Uncertainty Function (with orifice plates)
'For use with reservoir/headbox on lower floor level (UWRL) with orifice plates
'To determine uncertainty in single sample measurement, from Kline and
McClintock, 1953 with orifice plates
    Function SSUCdResT(Size, mA, deltaH, Q, Ptgage, Ht, P, Lc, W, Yplatform,
        Yramp, Yref, g, leak)
    Dim beta, Aorifice, Dorifice, Dpipe, pi, C, Calib As Double
    Dim wQ, wLc, wHt, wC, wW, wPtgage, wH, wP, wYplatform, wYramp, wYref,
        wmA, H
    Dim dQ, dH, dP, dYplatform, dYramp
    pi = 3.14159265359
    Lc = Lc / 12 'convert from inches to feet
    W = W / 12 'convert from inches to feet
'Calculate Q in Headbox (with orifice plates)
    If (Size = 4) Then
        C = 0.6197
```

```
        Aorifice = 1.5 ^ 2 * 3.14159 * 0.25 / 144
        beta = 1.5 / 4.026
        Q = (C * Aorifice * (2 * g * deltaH) ^ 0.5 / (1 - beta ^ 4) ^ 0.5) - leak
    ElseIf (Size = 8) Then
        C = 0.6106
        Aorifice = 5 ^ 2 * 3.14159 * 0.25 / 144
        beta = 5 / 7.981
        Calib = 1 '+ 0.0357131
        Q = (C * Aorifice * (2 * g * deltaH) ^ 0.5 / (1 - beta ^ 4) ^ 0.5) * Calib - leak
    ElseIf (Size = 20) Then
        C = 0.6029
        Aorifice = 14.016 ^ 2 * 3.14159 * 0.25 / 144
        beta = 14.016 / 19.25
        Q = (C * Aorifice * (2 * g * deltaH) ^ 0.5 / (1 - beta ^ 4) ^ 0.5)
        Calib = 1 - (0.000071079566 * Q ^ 2 - 0.002182705515 * Q +
      0.024449497333)
        Q = Q * Calib - leak
    Else: Q = "Check Meter!"
    End If
    H = Ptgage - Yref
    Ht = H + Q ^ 2 / (2 * g * W ^ 2 * (H + P + Yplatform - Yramp) ^ 2)
'Assign values from measurements
    wQ = 0.0025 * Q
    wLc = (1 / 32) / (2 * 12) '+- 1/64 of inch
```

```
    wW = (1 / 16) / 2 '+- 1/32 of inch

    wPtgage = 0.0005 / 2 '+-error in feet

    wYref = 0.0005 / 2 '+-error in feet

    wmA = 0.01 / 2 '+-error in mA

    wYramp = (1 / 32) / (2 * 12) '+- 1/64 of inch

    wYplatform = (1 / 32) / (2 * 12) '+- 1/64 of inch

'Calculate uncertainties

    wH = (((wPtgage / H) ^ 2 + (wYref * (-1) / H) ^ 2) ^ (1 / 2)) * H

'Calc uncertainty interval wHt by taking derivatives

    dH = 1 - (Q ^ 2) / (g * W ^ 2 * (H + P + Yplatform - Yramp) ^ 3)

    dQ = Q / (g * W ^ 2 * (H + P + Yplatform - Yramp) ^ 2)

    dP = -Q ^ 2 / (g * W ^ 2 * (H + P + Yplatform - Yramp) ^ 3)

    dYplatform = Q ^ 2 / (g * W ^ 2 * (H + P + Yplatform - Yramp) ^ 3)

    dYramp = Q ^ 2 / (g * W ^ 2 * (H + P + Yplatform - Yramp) ^ 3)

    wHt = (((wH * dH / Ht) ^ 2 + (wQ * dQ / Ht) ^ 2 + (wP * dP / Ht) ^ 2 +
        (wYplatform * dYplatform / Ht) ^ 2 + (wYramp * dYramp / Ht) ^ 2) ^ (1 / 2))
        * Ht

'% Uncertainty of single Cd value from arced labyrinth weir in headbox

    SSUCdResT = ((wQ / Q) ^ 2 + (-wLc / Lc) ^ 2 + (-27 / 8 * wHt / Ht) ^ 2) ^ (1 / 2)

    End Function



'Headbox Uncertainty Function (with calibrated mag-meter)

'To determine uncertainty in single sample measurement, from Kline and
McClintock, 1953 with mag-meter
```

```
'For use with reservoir/headbox on lower floor level (UWRL) with calibrated mag-
meter


    Function SSUCdResM(Size, Hertz, Q, Ptgage, Ht, P, Lc, W, Yplatform, Yramp,
        Yref, g, leak)

    Dim pi As Double

    Dim wQ, wLc, wHt, wC, wW, wPtgage, wH, wP, wYplatform, wYramp, wYref,
    wHz, H

    Dim dQ, dH, dP, dYplatform, dYramp

    pi = 3.14159265359

    Lc = Lc / 12 'convert from inches to feet

    W = W / 12 'convert from inches to feet

'Calculate Q in Headbox (with calibrated mag-meter)

    If (Size = 6) Then

        Q = ((Hertz * 1998.34 / 1000) - leak) / 448.381

        ElseIf (Size = "20M") Then

        Q = ((Hertz * 107.5) - leak) / 448.381

        Else: Q = "Check Meter!"

    End If

        H = Ptgage - Yref

        Ht = H + Q ^ 2 / (2 * g * W ^ 2 * (H + P + Yplatform - Yramp) ^ 2)

'Assign values from instrumentation

    wQ = 0.0025 * Q

    wLc = (1 / 32) / (2 * 12) '+- 1/64 of inch

    wW = (1 / 16) / 2 '+- 1/32 of inch
```

```
    wPtgage = 0.0005 / 2 '+-error in feet

    wYref = 0.0005 / 2 '+-error in feet

    wHz = 0.01 / 2 '+-error in Hertz

    wYramp = (1 / 32) / (2 * 12) '+- 1/64 of inch

    wYplatform = (1 / 32) / (2 * 12) '+- 1/64 of inch

'Calculate uncertainties

    wH = (((wPtgage / H) ^ 2 + (wYref * (-1) / H) ^ 2) ^ (1 / 2)) * H

'Calc uncertainty interval wHt by taking derivatives

    dH = 1 - (Q ^ 2) / (g * W ^ 2 * (H + P + Yplatform - Yramp) ^ 3)

    dQ = Q / (g * W ^ 2 * (H + P + Yplatform - Yramp) ^ 2)

    dP = -Q ^ 2 / (g * W ^ 2 * (H + P + Yplatform - Yramp) ^ 3)

    dYplatform = Q ^ 2 / (g * W ^ 2 * (H + P + Yplatform - Yramp) ^ 3)

    dYramp = Q ^ 2 / (g * W ^ 2 * (H + P + Yplatform - Yramp) ^ 3)

    wHt = (((wH * dH / Ht) ^ 2 + (wQ * dQ / Ht) ^ 2 + (wP * dP / Ht) ^ 2 +
        (wYplatform * dYplatform / Ht) ^ 2 + (wYramp * dYramp / Ht) ^ 2) ^ (1 / 2))
        * Ht

'% Uncertainty of single Cd value from arced labyrinth weir in headbox

    SSUCdResM = ((wQ / Q) ^ 2 + (-wLc / Lc) ^ 2 + (-27 / 8 * wHt / Ht) ^ 2) ^ (1 /
    2)

    End Function
```